International Journal of Bifurcation and Chaos, Vol. 6, No. 12B (1996) 2531–2555

TOPOLOGICAL ANALYSIS OF CHAOS IN EQUIVARIANT ELECTRONIC CIRCUITS

C. LETELLIER* and G. GOUESBET
LESP/URA CNRS 230, Place Emile Blondel,
76131 Mont Saint-Aignan Cedex, France,

N. F. RULKOV
Institute for Nonlinear Science,
University of California of San Diego, La Jolla, USA

Received February 21, 1996

Chaotic oscillations in an electronic circuit are studied by recording two time series simultaneously. The chaotic dynamics is characterized by using topological analysis. A comparison with two models is also discussed. Some prescriptions are given in order to take into account the symmetry properties of the experimental system to perform the topological analysis.

1. Introduction

Recently many papers have been devoted to global vector field reconstruction from a scalar time series [Packard *et al.*, 1980; Crutchfield & McNamara, 1987; Farmer & Sidorowitch, 1987; Agarwal *et al.*, 1990; Breeden & Hübler, 1990; Casdagli *et al.*, 1991; Giona *et al.*, 1991; Palus & Dvoràck, 1992; Gouesbet & Maquet; Gouesbet & Letellier, 1994; Brown *et al.*, 1995; Letellier *et al.*, 1995a, 1995b]. In particular, the extraction of a set of equations which model the dynamics has been successfully achieved from experimental data generated by a Belousov–Zhabotinskii reaction [Brown *et al.*, 1995] or by a copper electrodissolution [Letellier *et al.*, 1995a, 1995b]. Nevertheless, an important question is how to introduce an equivariance property in the reconstructed vector field and, therefore determine the symmetry properties of a system from a scalar time series? This issue is significant because it has been shown that, in the presence of symmetry, the different variables required to span the original phase space are not necessarily equivalent from the reconstruction method point of view [King & Stewart, 1992]. In particular, the dynamics induced by different variables may be topologically different. This problem principally arises when a system may be described by equivariant or invariant variables as well exemplified by the Lorenz system [Letellier & Gouesbet, 1996].

For instance, it has been shown that an equivariant variable always induces phase portraits which present an inversion symmetry. This symmetry may be different than on the original attractor as in the case of the Lorenz system where the original attractor presents an axial symmetry [Letellier *et al.*, 1994]. As stated by King and Stewart [King & Stewart, 1992], a phase portrait may be reconstructed with an axial symmetry by using two scalar time series, one equivariant and one invariant. Consequently, it is of importance to correctly define the nature of the equivariance when one likes to perform a precise reconstruction of a set of equations.

*E-mail: letellie@coria.fr

This paper is devoted to the topological analysis of experimental data generated by an electronic circuit [Rulkov *et al.*, 1992, 1994] where symmetry properties are present. Section 2 is devoted to a brief review concerning symbolic dynamics with many symbols. Section 3 discusses the topological analysis of the experimental data which are given under the form of two time series recorded simultaneously. Comparisons with Chua's system and a model proposed by one of us is given in Sec. 4. Section 5 is the conclusion.

2. Symbolic Plane

In order to achieve a topological analysis of the attractor generated by the electronic circuit, we use common concepts from the topological characterization theory such as templates, linking numbers and symbolic planes. We shall have to characterize the population of periodic orbits of a quartic map, i.e. constituted by four monotonic branches. Consequently, following recent papers [Fang, 1994; Fa-Geng, 1994; Duan *et al.*, 1994], we have to introduce the symbolic coordinates.

In the case of a quartic map (Fig. 1), three critical points C_i define a partition of the attractor and any trajectory may be encoded by using:

$$\sigma_n = \begin{cases} 0 & \text{if} \quad x_n < C_1 \\ 1 & \text{if} \quad C_1 < x_n < C_2 \\ 2 & \text{if} \quad C_2 < x_n < C_3 \\ 3 & \text{if} \quad C_3 < x_n \end{cases} \tag{1}$$

where σ_n is the code of the nth intersection of the trajectory with a Poincaré plane.

Thus, a chaotic trajectory forms a string

$$s = \ldots \sigma_{-3}\sigma_{-2}\sigma_{-1}\sigma_0\sigma_1\sigma_2\sigma_3 \ldots$$

where σ_0 is the present, σ_{-i} the past and σ_i the future ($i > 0$). Let s_f be the substring $\{\sigma_i\}_{i=1}^{D}$ on the future and s_p the substring $\{\sigma_{-i}\}_{i=0}^{D-1}$ on the past in which D may be taken as equal to 16.

The forward symbolic coordinate reads as [Fang, 1994]:

$$\alpha(s_f) = \sum_{i=1}^{D} \frac{\mu_i}{4^i} \tag{2}$$

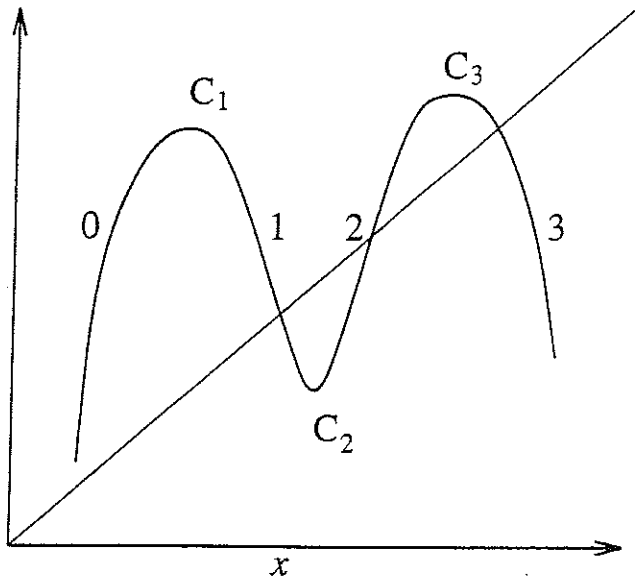

Fig. 1. A quartic map.

where

$$\mu_i = \begin{cases} 0 \\ 2 \\ 2 \\ 0 \end{cases} \quad \text{for} \quad \sigma_i = \begin{cases} 0 \\ 1 \\ 2 \\ 3 \end{cases} \tag{3}$$

$$\text{if} \quad \sum_{j=1}^{i} \sigma_i = 0 \ (\text{mod } 2)$$

and

$$\mu_i = \begin{cases} 3 \\ 1 \\ 1 \\ 3 \end{cases} \quad \text{for} \quad \sigma_i = \begin{cases} 0 \\ 1 \\ 2 \\ 3 \end{cases} \tag{4}$$

$$\text{if} \quad \sum_{j=1}^{i} \sigma_i = 1 \ (\text{mod } 2)$$

This forward coordinate $\alpha(s_f)$ gives the multimodal order of the symbolic sequences following the natural order of the real numbers on the interval [0, 1]. Then, a symbolic sequence W_1 is said to be implied by a sequence W_2 if $\alpha_{W_1} < \alpha_{W_2}$. As a period-$p$ orbit may be encoded by p symbolic sequences W_i, the so-called orbital sequence (W) is the cyclic permutation W_i implying the $(p-1)$ others. By ordering the forward coordinates of the orbital sequences (W)'s, we obtain the forcing order of the orbits. For instance, the orbit encoded by (W_2) forces the orbit encoded by (W_1) if $\alpha(W_1) < \alpha(W_2)$. All orbital sequences of orbits whose period

Table 1. Forward coordinates associated with orbital sequences of orbits whose period is less than 5.

(W)	$\alpha(W)$	(W)	$\alpha(W)$
1	0.3999	320	0.8615
10	0.4705	3203	0.8627
1011	0.4747	3202	0.8638
101	0.4761	3201	0.8705
100	0.4923	3200	0.8715
1001	0.4941	3100	0.8784
1000	0.4980	3101	0.8793
2000	0.5019	3102	0.8862
2001	0.5058	3103	0.8871
200	0.5079	310	0.8888
201	0.5230	311	0.8923
2011	0.5254	3113	0.8941
2010	0.5291	3112	0.8949
20	0.5333	3111	0.9019
21	0.5882	3110	0.9027
2120	0.5914	3120	0.9098
2110	0.5960	3121	0.9105
2111	0.5992	3122	0.9176
211	0.6031	3123	0.9182
210	0.6153	312	0.9206
2101	0.6196	313	0.9230
2100	0.6225	3133	0.9254
2200	0.6274	3132	0.9260
2201	0.6303	31	0.9333
220	0.6349	30	0.9411
221	0.6461	3031	0.9416
2211	0.6509	3032	0.9490
2210	0.6536	3033	0.9494
2220	0.6588	303	0.9523
2221	0.6614	302	0.9538
2	0.6666	3023	0.9568
3	0.7999	3022	0.9571
32	0.8235	3021	0.9647
3233	0.8249	3020	0.9649
323	0.8253	3010	0.9725
322	0.8307	3011	0.9727
3223	0.8313	3012	0.9803
3222	0.8326	3013	0.9805
3221	0.8392	301	0.9841
3220	0.8404	300	0.9846
3210	0.8470	3003	0.9882
3211	0.8482	3002	0.9883
3212	0.8549	3001	0.9960
3213	0.8560	3000	0.9961
321	0.8571		

is less than 5 are reported in Table 1 with the associated forward coordinates.

Nevertheless, a quartic map for which the creation of periodic orbits under the variation of a control parameter is given by the forcing order is rather a marginal case. As shown by many workers [Fang, 1994, Fa-Geng, 1994; Dutertre, 1995], a quartic map does not necessarily exhibit the forcing order given by the forward coordinate and, consequently, in order to have a good knowledge of the population of periodic orbits, a kneading sequence has to be associated with each critical point. Such kneading sequences are determined by using a symbolic plane spanned by the forward coordinate $\alpha(s_f)$ and the backward coordinate $\beta(s_p)$. The backward coordinate reads as:

$$\beta(s_p) = \sum_{i=1}^{D} \frac{\nu_i}{4^i} \tag{5}$$

where

$$\nu_i = \begin{cases} 3 \\ 1 \\ 1 \\ 3 \end{cases} \quad \text{for} \quad \sigma_{-i+1} = \begin{cases} 0 \\ 1 \\ 2 \\ 3 \end{cases} \tag{6}$$

$$\text{if} \quad \sum_{j=1}^{i} (1 - \sigma_{-i}) = 0 \pmod 2$$

and

$$\nu_i = \begin{cases} 0 \\ 2 \\ 2 \\ 0 \end{cases} \quad \text{for} \quad \sigma_{-i+1} = \begin{cases} 0 \\ 1 \\ 2 \\ 3 \end{cases} \tag{7}$$

$$\text{if} \quad \sum_{j=1}^{i} (1 - \sigma_{-i}) = 1 \pmod 2$$

The knowledge of the pruning fronts exhibited on this symbolic plane allows one to determine the kneading sequences associated with each critical point [Fang, 1994; Fa-Geng, 1994]. Indeed, it has been shown that the population of periodic orbits may be determined from the knowledge of the kneading sequences K_i associated with the critical points C_i [Fa-Geng, 1994]. Then, for such a general quartic map as displayed in Fig. 1, admissible orbital sequences (W) whose cyclic permutations are W_i must satisfy the conditions as follows.

Starting from the first iterate of a critical point C_i, we generate a kneading sequence K_i which is

Table 2. Forward coordinates associated with each periodic orbit following the descending order.

(W)	$\alpha(W)$	(W)	$\alpha(W)$
0001	0.0077	0331	0.1945
0002	0.0078	0332	0.1960
0003	0.0155	0333	0.2023
0013	0.0156	0323	0.2039
0012	0.0233	0322	0.2101
0011	0.0235	0321	0.2117
001	0.0307	032	0.2153
002	0.0317	031	0.2222
0021	0.0389	0311	0.2256
0022	0.0392	0312	0.2274
0023	0.0466	0313	0.2334
0033	0.0470	03	0.2352
0032	0.0544	13	0.2666
0031	0.0549	1312	0.2723
003	0.0615	1311	0.2745
013	0.0634	131	0.2769
0131	0.0700	132	0.2857
0132	0.0705	1321	0.2879
0133	0.0778	1322	0.2901
0123	0.0784	1323	0.2957
0122	0.0856	1333	0.2980
0121	0.0862	1332	0.3035
012	0.0923	1331	0.3058
011	0.0952	133	0.3076
0111	0.1011	123	0.3174
0112	0.1019	1231	0.3190
0113	0.1089	1232	0.3215
0103	0.1098	1233	0.3268
0102	0.1167	1223	0.3294
01	0.1176	1222	0.3346
02	0.1333	1221	0.3372
0203	0.1400	122	0.3384
0213	0.1411	121	0.3492
0212	0.1478	1211	0.3501
0211	0.1490	12	0.3529
021	0.1538	1	0.3999
022	0.1587	2	0.6666
0221	0.1634	2223	0.6692
0222	0.1647	2233	0.6745
0223	0.1712	223	0.6769
0233	0.1725	233	0.6984
0232	0.1789	2333	0.7003
0231	0.1803	23	0.7058
023	0.1846	3	0.7999
033	0.1904		

associated with a symbolic coordinate $\alpha(K_i)$. For the general quartic map with three critical points, we have three kneading sequences K_1, K_2 and K_3 associated with three symbolic coordinates $\alpha_1 = \alpha(K_1)$, $\alpha_2 = \alpha(K_2)$ and $\alpha_3 = \alpha(K_3)$, respectively.

Now let (W) be the orbital sequence of a period-p orbit ξ. The orbit ξ is actually present within the attractor if its p cyclic permutations

$$W_i = \sigma_i\sigma_{i+1}\ldots\sigma_p\sigma_1\ldots\sigma_{i-1}\,,$$

rewritten as

$$W_i = W_i^*\sigma_{i-1}$$

where W_i^* is the string of the $(p-1)$ first symbols satisfy the conditions

$$\begin{cases} \alpha(K_1) > \alpha(W_i) & \text{if} \quad \sigma_{i-1} = 0 \quad \text{or} \quad \sigma_{i-1} = 1 \\ \alpha(K_2) < \alpha(W_i) & \text{if} \quad \sigma_{i-1} = 1 \quad \text{or} \quad \sigma_{i-1} = 2 \\ \alpha(K_3) > \alpha(W_i) & \text{if} \quad \sigma_{i-1} = 2 \quad \text{or} \quad \sigma_{i-1} = 3 \end{cases} \tag{8}$$

Thus, the knowledge of the three forward coordinates α_i allows one to completely determine the population of unstable periodic orbits. From the symbolic plane, knowing α_1 and α_3, the kneading sequences K_1 and K_3 may be obtained from Table 1 since they are determined by the so-called ascending order [Fa-Geng, 1994]. Conversely, knowing α_2, the kneading sequence K_2 is given by Table 2 since it is determined by the descending order [Fa-Geng, 1994].

3. Topological Analysis of the Electronic Circuit

The system is an electronic circuit whose block diagram is shown in Fig. 2. The circuit consists of a nonlinear amplifier N which transforms the input voltage $X(t)$ into the output $\alpha f(X)$ [Rulkov *et al.*, 1992]. The parameter α characterizes the gain of N around $X = 0$. The nonlinear amplifier has a linear feedback which contains a series connection to a low pass filter (RC') and to an LC resonance branch. It has been shown that this circuit can exhibit a transition from periodic oscillations to chaos via period-doubling cascades, intermittency and crises of chaotic attractors [Volkovski & Rulkov, 1988]. In our topological analysis, we investigated the two values of the parameter α studied in [Brown *et al.*, 1995]. These values ($\alpha = 17.4$ and 18.9) correspond to the chaotic attractors which appear after a period-doubling cascade. Each chaotic

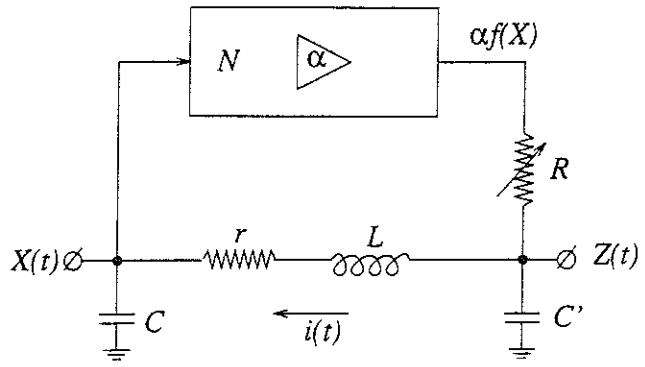

Fig. 2. A schematic diagram of the electronic circuit here studied. For this circuit, data are collected at $R = 3.38$ kΩ, $L = 145$ mH, $C = 343$ nF, $C' = 225$ nF, $r = 347\ \Omega$, with a sampling period of 20 μs and $\alpha = 17.4$ and 18.9.

signal $X(t)$, measured from the capacitor C, has been amplified, and the digitized signal $X(n\delta t)$ is the first scalar time series under study. A second signal is simultaneously recorded.

The method of time delays was used to reconstruct phase space vectors reading as:

$$\{X(n\delta t),\ X(n\delta t + \tau), \ldots,\ X(n\delta t + (d_E - 1)\tau)\} \tag{9}$$

In order to find the embedding delay τ and the embedding dimension d_E, Brown *et al.* [1995] used the methods of average mutual information [Fraser & Swinney, 1986] and false near neighbors [Kennel, 1992]. The results of the calculations for both values of α indicate that the correct embedding time is $\tau = 10\delta t$ and the correct embedding dimension is $d_E = 3$.

As the embedding dimension is found to be equal to 3, the attractor may be embedded in the state space spanned by the (U, V, W)-coordinates which reads as:

$$\begin{cases} U = X(n\delta t) \\ V = X(n\delta t + \tau) \\ W = X(n\delta t + 2\tau) \end{cases} \tag{10}$$

The system being considered possesses symmetry properties which are evidenced by the symmetry of the nonlinear function, $f(X) = -f(-X)$. Chaos in the circuit appears as a result of a period-doubling cascade process from a pair of mutually symmetric limit cycles. For $\alpha = 17.4$, two attractors A^- and A^+, one being symmetric of the other, co-exist. Consequently, two period-doubling cascades may be observed depending on the initial conditions. A boundary crisis is hereafter observed and a larger symmetric attractor A^S, which is also called the double scroll attractor, is found for $\alpha = 18.9$. The topological analysis will be performed for one of the attractors of the bistable regime ($\alpha = 17.4$) and for the larger symmetric attractor ($\alpha = 18.9$).

3.1. *The attractor of the bistable regime*

As previously indicated, two time series are simultaneously recorded. Firstly, we will achieve the topological analysis of the X-induced attractor A_X^+. The attractor reconstructed from the second variable Z, here called A_Z^+ will hereafter be characterized.

3.1.1. *Orbit spectrum*

For $\alpha = 17.4$, depending on the initial conditions, the asymptotic motion settles down on to one of the two attractors which are symmetrical one with respect to the other. One of those is displayed in Fig. 3.

This attractor is studied via a Poincaré section P defined by

$$P \equiv \{(U, V) \in \mathbb{R}^2 | U = 4.0,\ \dot{U} < 0\} \tag{11}$$

A first-return map is hereafter built and displayed in Fig. 4. Three monotonic branches separated by two critical points given by

$$\begin{cases} C_1 = 1.65 \\ C_2 = -0.70 \end{cases} \tag{12}$$

are exhibited.

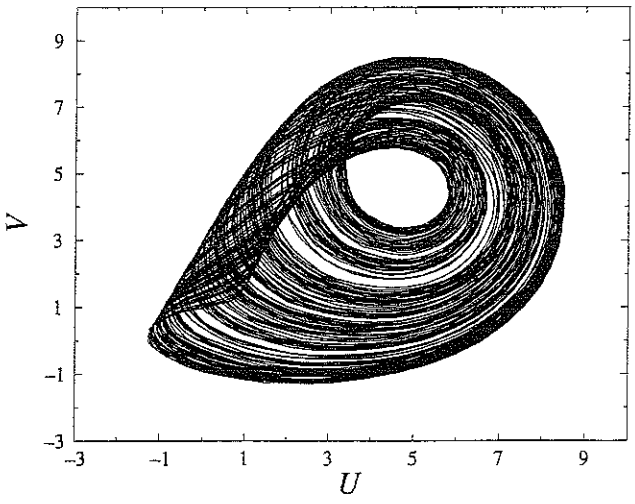

Fig. 3. Plane projection of the attractor A_X^+.

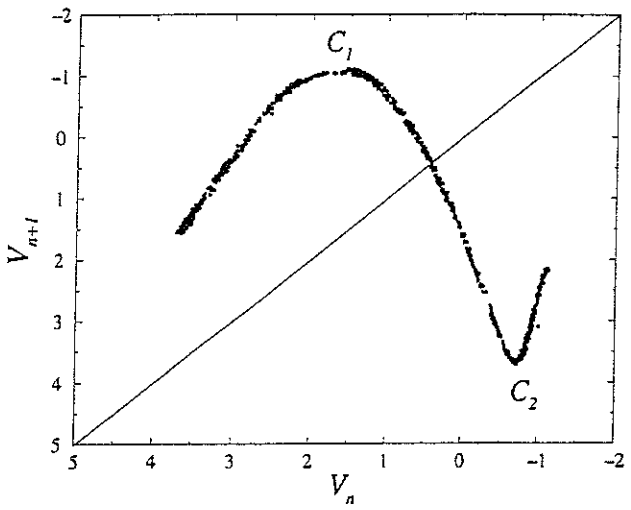

Fig. 4. First-return map to the Poincaré section P computed with the V-coordinate.

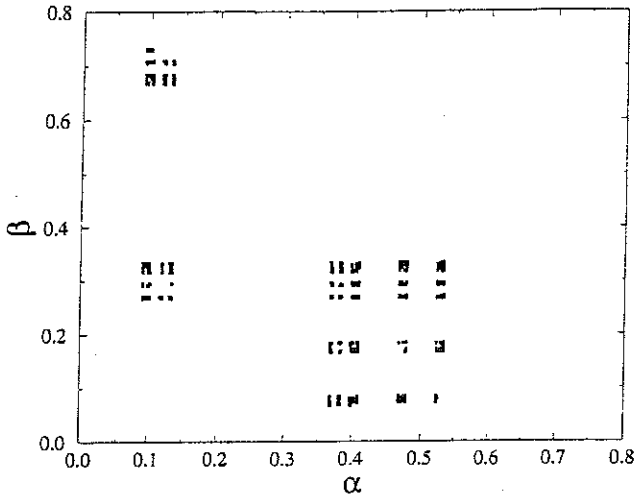

Fig. 5. Symbolic plane of the attractor A_X^+.

Periodic orbits are extracted from the Poincaré section P and encoded following the generating partition which reads as:

$$\begin{cases} 0 & \text{if} \quad V_n > C_1 \\ 1 & \text{if} \quad C_2 > V_n > C_1 \\ 2 & \text{if} \quad C_2 > V_n \end{cases} \tag{13}$$

The corresponding population of periodic orbits is reported in Table 3.

Such an orbit spectrum may be checked by computing the symbolic plane (Fig. 5). The ascending pruning front, associated with the critical point C_1, is located at $\alpha_1 = 0.5328$ while the descending pruning front, associated with the critical point C_2, is located at $\alpha_2 = 0.0917$. From these symbolic coordinates and Tables 1 and 2, the kneading sequences are found to be written as

$$\begin{cases} K_1 = (\overline{20}) \\ K_2 = (\overline{012}) \end{cases} \tag{14}$$

One may check in Tables 1 and 2 that all periodic orbits extracted from the attractor A_X^+ are found to be forced by the kneading sequence K_1 following the ascending order and by the kneading sequence K_2 following the descending order.

Table 3. Population of periodic orbits embedded within the attractor A^+ for $\alpha = 17.4$.

Period	(W)	Period	(W)
1	1		20111
2	10		20101
3	201		20100
	101	6	101110
4	1011		101111
	2011		201101
	2010		201110
5	10111		201010
	10110		201011
	20110		

3.1.2. *Template*

As the first-return map is constituted by three monotonic branches, the template synthetizing the topology of the attractor A_X^+ exhibits three stripes. Starting from a mask of this attractor (Fig. 6) a stripe, labeled 0, is found without any local torsion and is to be associated with the increasing branch 0.

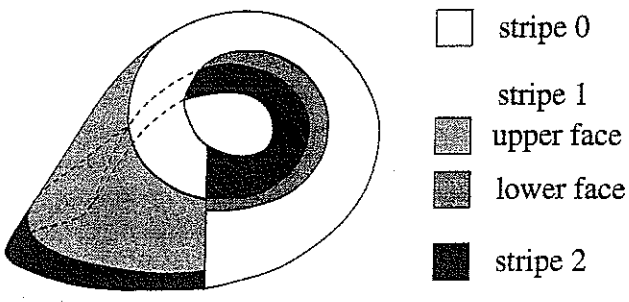

Fig. 6. Mask of the attractor A_X^+.

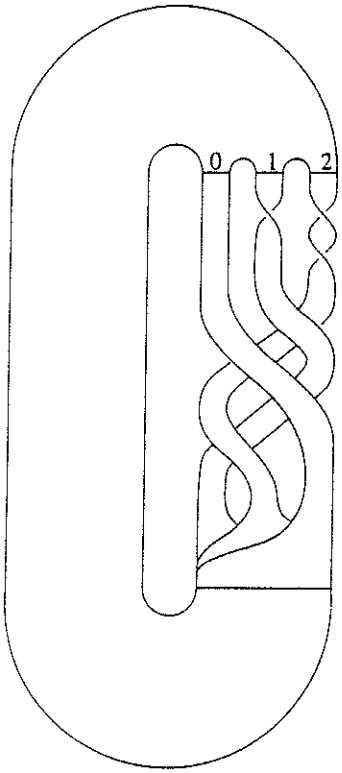

Fig. 7. Template of the attractor A^+.

A second stripe, labeled 1, which undergoes a negative π-twist, corresponds to branch 1. The third stripe, labeled 2, presents two negative π-twists and is associated with the increasing branch. From this mask, the template is extracted and found to be defined by a linking matrix which reads as:

$$M = \begin{pmatrix} 0 & -1 & -1 \\ -1 & -1 & -2 \\ -1 & -2 & -2 \end{pmatrix} \tag{15}$$

where the on-diagonal elements M_{ii} give the number of π-twists on the ith stripe and the off-diagonal elements M_{ij} give the sum of the oriented crossings between the ith stripe and the jth stripe. The template is displayed in Fig. 7.

This template may be checked by counting the linking numbers on the plane projections of a few couples of periodic orbits. The couples $(201, 1)$ and $(2010, 201)$ are displayed in Fig. 8. The linking numbers $L(201, 1)$ and $L(2010, 201)$ are found to be equal to -1 and -5, respectively. These linking numbers are equal to the ones predicted by the template. The template is therefore validated.

3.1.3. *Attractor induced by the second time series*

The second time series is recorded as indicated in Fig. 2. From the principle of the redundancy of information within a nonlinear dynamical system, each variable is equivalent, i.e. all attractors reconstructed from each variable are equivalent. Nevertheless, we have shown that there exist some pathological cases where this principle is not valid when the embedding dimension is equal to the dimension of the original phase space [Letellier & Gouesbet,

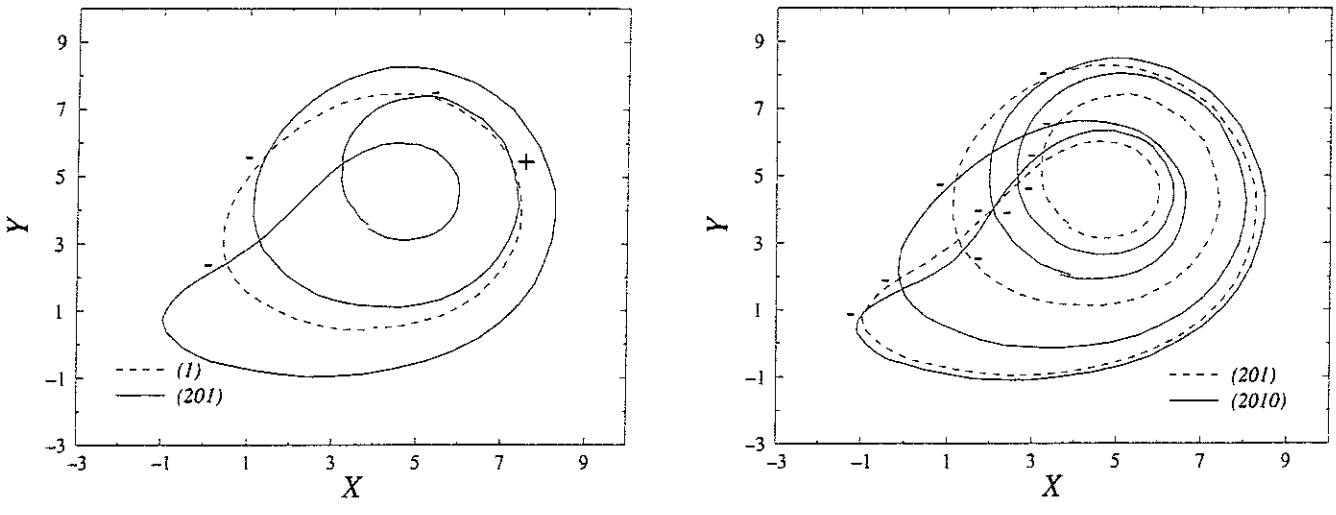

Fig. 8. Plane projection of two couples of periodic orbits. (a) $L(201, 1) = \frac{1}{2}[-3 + 1] = -1$. (b) $L(2010, 201) = \frac{1}{2}[-10] = -5$.

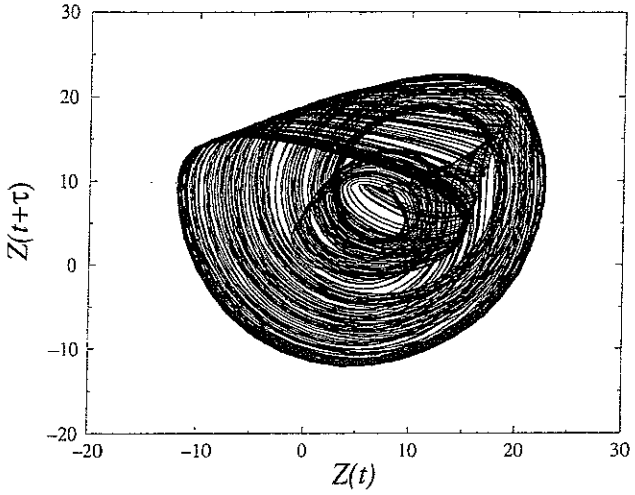

Fig. 9. Attractor A_Z^+ reconstructed from the second time series. $\tau = 9\delta t$.

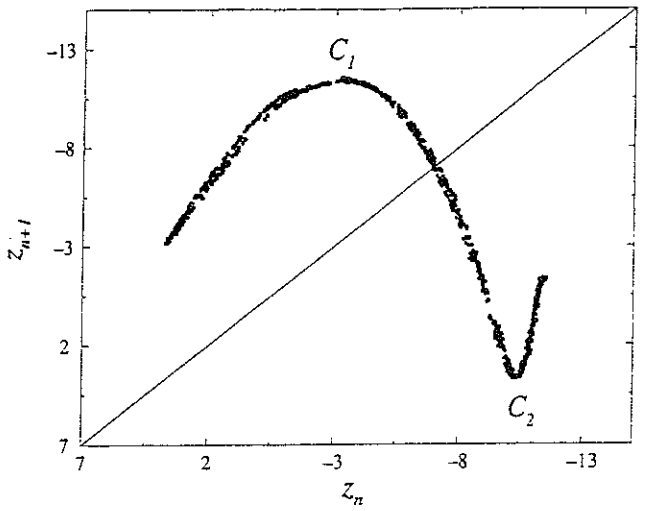

Fig. 10. First-return map to the Poincaré section P. It looks rather similar to the one associated with the X-induced attractor A_X^+.

1996]. As stated by Takens [1981], an embedding dimension which gives a diffeomorphical equivalence must be fixed to be equal to at least $2D_2 + 1$ where D_2 is the correlation dimension estimated by algorithms as the one proposed by Grassberger and Proccacia [1983]. Nevertheless, such a condition is rather severe and would prevent the use of topological characterization which is restricted to $3D$-spaces. Moreover, King and Stewart [King & Stewart, 1992] have shown that the Takens' theorem must be extended to preserve symmetry properties.

Consequently, it may not be surprising that two attractors reconstructed from two different variables of a single system may be found to be different when the embedding dimension is taken to be equal to the dimension of the original phase space. The case of our experimental electronic circuit seems to correspond to such a pathological case. Indeed, the Z-induced attractor is displayed in Fig. 9 and looks rather different than the one induced by the X-time series.

The time delay τ is taken to be equal to $9\delta t$. This value has been fixed to a smaller value than the one used with the first time series to obtain a hole in the middle of the attractor. Such a hole is of crucial importance to safely define a Poincaré section. With this time delay, the Poincaré section P is defined by

$$P = \{(Z(t),\, Z(t+2\tau) \in \mathbb{R}^2 | Z(t+\tau) = 12.3\,, \quad Z(t) < 4.0,\, \dot{Z}(t+\tau) > 0\} \quad (16)$$

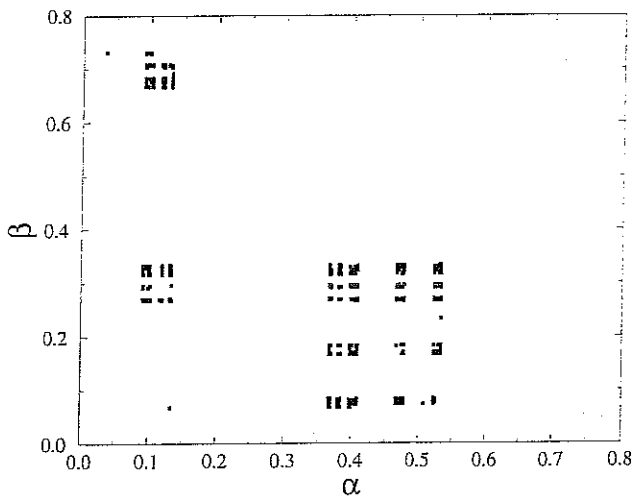

Fig. 11. Symbolic plane of the Z-induced attractor.

The first return map to this Poincaré section is computed with the $Z(t)$ variable and displayed in Fig. 10. As for the X-induced attractor, the first-return map exhibits three monotonic branches separated by two critical points given by:

$$\begin{cases} C_1 = -3.212 \\ C_2 = -10.380 \end{cases} \quad (17)$$

The symbolic plane is hereafter computed (Fig. 11). The kneading forward coordinates are found to be:

$$\begin{cases} \alpha_1 = 0.5328 \\ \alpha_2 = 0.33 \end{cases} \quad (18)$$

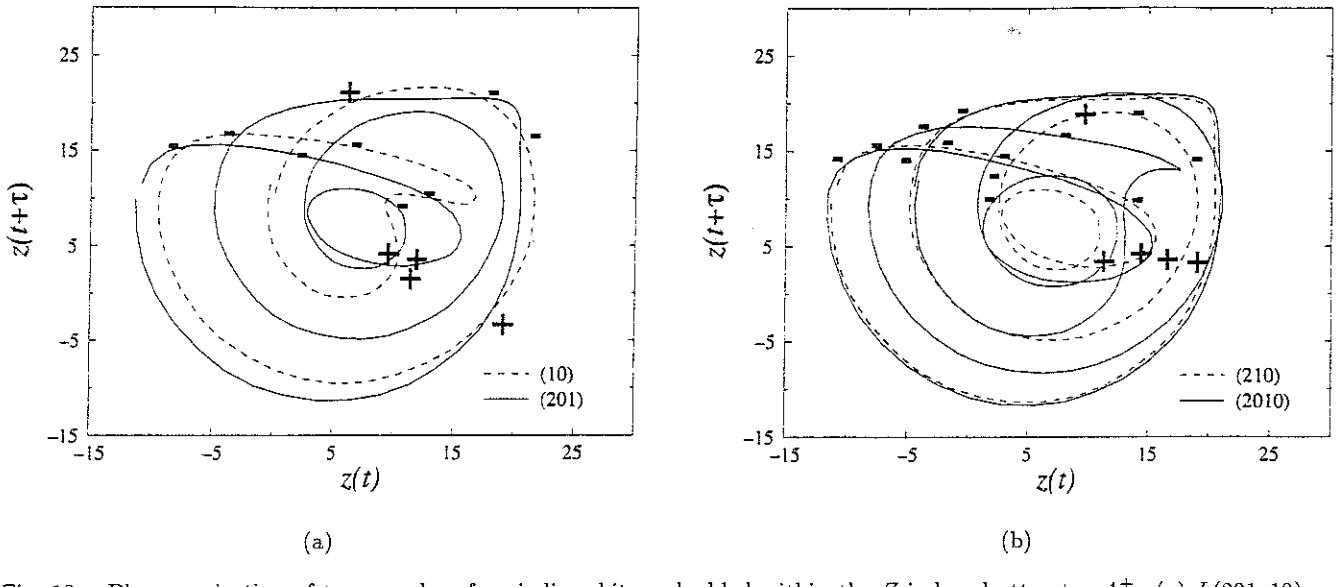

Fig. 12. Plane projection of two couples of periodic orbits embedded within the Z-induced attractor A_Z^+. (a) $L(201, 10) = \frac{1}{2}[-8 + 4] = -2$. (b) $L(2011, 201) = \frac{1}{2}[5 - 13] = -4$.

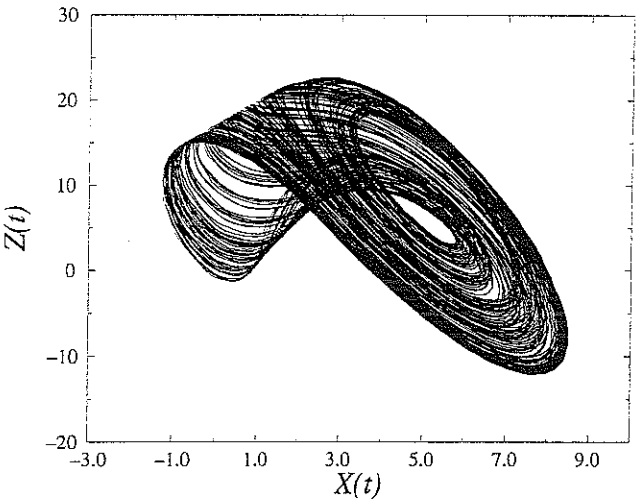

Fig. 13. Plane projection of the attractor reconstructed from the two time series $X(t)$ and $Z(t)$.

From Table 1 and Table 2, they are found to be associated with kneading sequences which may be written as:

$$\begin{cases} K_1 = (\overline{20}) \\ K_2 = (\overline{0021}) \end{cases} \tag{19}$$

respectively. The kneading sequence K_1, associated with the ascending order, is the same for the two different attractors. Nevertheless, the kneading sequence K_2, associated with the descending order, implies that the second critical point C_2 of the Z-induced attractor allows more orbits than the second critical point of the X-induced attractor. It is not impossible that such a difference may be generated by the time delay change (such a dependence could be completely studied in future works).

The Z-induced attractor looks rather complicated and we have to check if its topology is compatible with the template of the X-induced attractor. In order to check the topological equivalence between the attractors A_X^+ whose template is defined by the linking matrix (15) and A_Z^+, we evaluate the linking numbers between a few couples of orbits. We found that

$$\begin{cases} L(2010, 1) &= -2 \\ L(2011, 1) &= -2 \\ L(201, 10) &= -2 \\ L(2011, 201) &= -4 \\ L(2010, 201) &= -4 \end{cases} \tag{20}$$

Two plane projections associated with two of the linking numbers are displayed in Fig. 12. All of these linking numbers are correctly predicted by a linking matrix which reads as:

$$M_{A_Z} = \begin{pmatrix} 0 & -1 & -1 \\ -1 & -1 & -2 \\ -1 & -2 & 0 \end{pmatrix} \tag{21}$$

Consequently, there is no topological equivalence between the X-induced attractor A_X^+ and the Z-induced attractor A_Z^+. Indeed, the third stripe of A_Z^+ presents no local torsion while the third stripe of A_X^+ undergoes two negative π-twists. Such a

case of lack of equivalence has been observed on the Burke'n Shaw system [Letellier *et al.* 1996]. Once again, the principle of the equivalence between two variables of a single system is not checked. Moreover, Mindlin and Solari [1995] have shown that an embedding may depend on the used time delay.

Nevertheless, it seems that we could define the topology of the true dynamics underlying the electronic circuit. We know that the embedding dimension is equal to 3. Three independent variables are therefore required to span a reconstructed phase space. We already have two scalar time series which may be viewed as having been obtained from two variables of the reconstructed phase space. In order to obtain a third variable, we may use $X(t+\tau)$ or $Z(t+\tau)$. In this section, we will denote this third variable by $w(t)$.

A XZ-plane projection of the attractor reconstructed from the two time series is displayed in Fig. 13. The attractor looks rather similar to the X-induced attractor.

A Poincaré section is defined by

$$P_{XZ} = \{(X(t),\, w(t)) \in \mathbb{R}^2 | X = 5.0,\, \dot{X} < 0\} \quad (22)$$

A first-return map to this Poincaré section is computed and displayed in Fig. 14. Three monotonic branches are found to be separated by two critical points given by:

$$\begin{cases} C_1 = 0.32 \\ C_2 = -4.64 \end{cases} \quad (23)$$

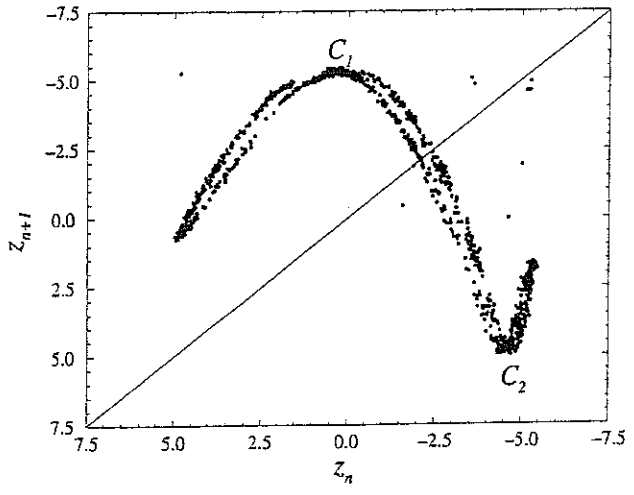

Fig. 14. First-return map to the Poincaré section P_{XZ}.

The symbolic plane is computed and the kneading forward coordinates are found to be equal to

$$\begin{cases} \alpha_1 = 0.5333 \\ \alpha_2 = 0.0328 \end{cases} \quad (24)$$

with the associated kneading sequences

$$\begin{cases} K_1 = (\overline{20}) \\ K_2 = (\overline{002}) \end{cases} \quad (25)$$

Once again, the kneading sequence K_1 agrees with the one found on the X-induced attractor while the second kneading sequence K_2 is found to be different. By computing linking numbers, we found that the topology of this attractor is characterized by a linking matrix which reads as:

$$M_{XZ} = \begin{pmatrix} 0 & 0 & 0 \\ 0 & +1 & +1 \\ 0 & +1 & +2 \end{pmatrix} \quad (26)$$

This linking matrix seems very different from the linking matrix of Eq. (15). Nevertheless, as expected when taking into account symmetry properties, all local torsions designated by the diagonal elements are found with an inverse sign when compared to Eq. (15). The off-diagonal elements however are found to be different due to the use of the standard insertion convention [Melvin & Tufillaro, 1991], i.e. it is not actually significant. Let us further comment on the issue. We have used a space spanned by the coordinates (X, Z, w). Let us consider that this triplet of variables defines a right-handed system. We have no deep physical reason to choose such a system, and we could use the space spanned by (X, w, Z) as well. For instance, if we consider the Rössler system described by the three variables (x, y, z), the dynamics is preserved under the map Φ: $(x, y, z) \to (z, y, x)$. Nevertheless, if the original space is considered as right-handed, the new space spanned by (z, y, x) is not. The immediate consequence is that all oriented crossings are mapped to their opposite (Fig. 15). The attractor reconstructed in the new space spanned by (z, y, x) is then characterized by an opposite template although the dynamical behavior is the same as on the original attractor. Similarly, we are not allowed to say that the dynamical behavior of the XZ-induced attractor is different from the X-induced attractor. Indeed, the difference between Eqs. (15) and (26) is due to the fact that all oriented crossings for the present attractor are inversed with respect to those of the X-induced attractor.

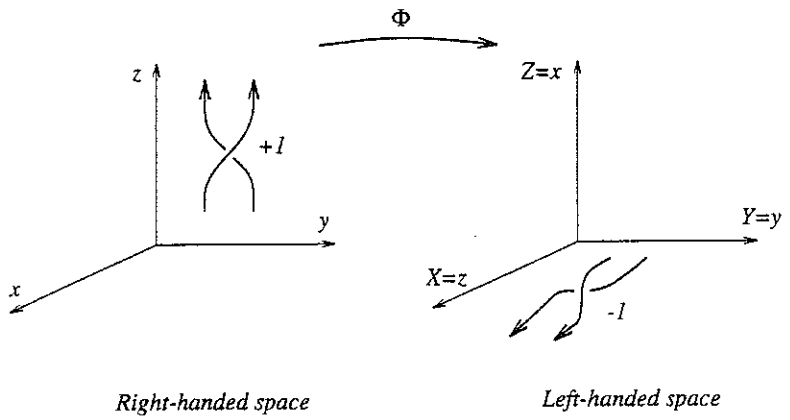

Fig. 15. An oriented crossing in a right-handed system is mapped to its opposite crossing in a left-handed system.

Therefore the topology of the true dynamics is likely to be the one of the X-induced attractor in so far as it is more robust than the topology of the Z-induced attractor. The Z-time series could therefore be pathological.

3.2. *The larger symmetric attractor*

3.2.1. *The symmetry of the attractor*

After a boundary crisis, the asymptotic motion settles down to a larger symmetric attractor which is displayed in Fig. 16 for $\alpha = 18.9$. The topological analysis of such an attractor with symmetry properties requires a specific procedure [Letellier *et al.* 1994] [Letellier & Gouesbet, 1996]. Indeed, when a system is equivariant, a pertinent dynamical information may be obtained by working in a fundamental domain $\mathcal{D}$. Then, as a first step to the analysis, we have to define the nature of the symmetry properties of the attractor. Let us recall that the attractor is embedded in a space spanned by the delay coordinates from the equivariant variable $x(t)$.

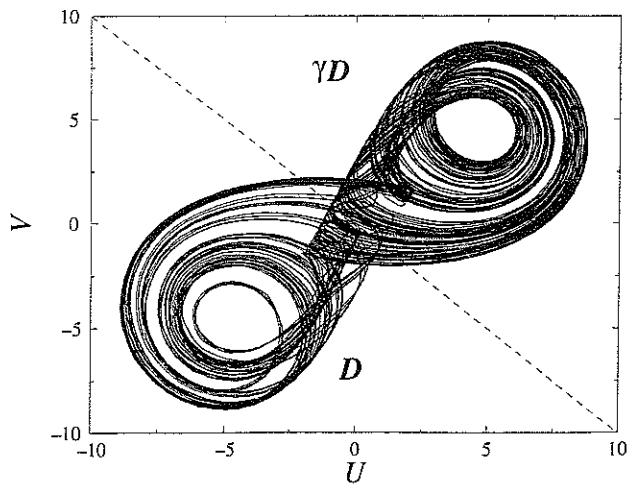

Fig. 16. Plane projection of the symmetric attractor.

As the attractor possesses symmetry properties, the vector field generating this attractor is equivariant, i.e.

$$f(\gamma x) = \gamma f(x)$$

where γ is the matrix defining the equivariance. An equivariant variable is here mapped to its opposite under the action of the γ-matrix. An invariant variable is invariant under the action of the γ-matrix. The symmetry properties of a reconstructed attractor depend crucially on the nature of the variable used to build a set of coordinates which may be indifferently taken as delay coordinates, derivative coordinates or principal components [Gibson *et al.*, 1992]. If a phase space is reconstructed from an invariant variable, the induced attractor possesses no symmetry properties. Conversely, if an equivariant variable is used, each coordinate derived from it is equivariant too. Consequently, all coordinates are equivariant and the γ-matrix of the reconstructed attractor reads as:

$$\gamma = \begin{pmatrix} -1 & 0 & 0 \\ 0 & -1 & 0 \\ 0 & 0 & -1 \end{pmatrix} \qquad (27)$$

defining an inversion symmetry.

It has been shown that in the presence of an inversion symmetry, the topological characterization may be conveniently achieved by working with

unsigned fundamental linking numbers [Letellier & Gouesbet, 1996]. Let us recall this specific procedure starting from the x-variable of the Lorenz system.

3.2.2. *Topological analysis in presence of the inversion symmetry*

The Lorenz system reads as:

$$\begin{cases} \dot{x} = \sigma(y - x) \\ \dot{y} = Rx - y - xz \\ \dot{z} = -bz + xy \end{cases} \tag{28}$$

in which we use a control parameter vector (R, σ, b) = (28, 10, 8/3) for which the asymptotic motion settles down on to a strange chaotic attractor [Lorenz, 1963]. The vector field f is equivariant with an equivariant matrix which reads as:

$$\gamma_L = \begin{pmatrix} -1 & 0 & 0 \\ 0 & -1 & 0 \\ 0 & 0 & 1 \end{pmatrix} \tag{29}$$

defining an axial symmetry.

The original attractor is characterized by a fundamental template whose linking matrix reads as:

$$M_L = \begin{pmatrix} 0 & 0 \\ 0 & +1 \end{pmatrix} \tag{30}$$

and is associated with the fundamental domain, i.e. a wing of the attractor [Letellier *et al.* 1994].

In the presence of a symmetry, the dynamics must be projected on a fundamental domain to obtain a convenient analysis. Thus, the dynamical behavior must be analyzed by using a Poincaré set rather than a Poincaré section. In the case of the attractor induced by the x variable, we use a state space spanned by derivative coordinates according to:

$$\begin{cases} X = x \\ Y = \dot{x} \\ Z = \ddot{x} \end{cases} \tag{31}$$

Let us recall that it has been shown that the delay coordinates are equivalent to the derivative coordinates [Gibson *et al.* 1992]. The Poincaré set P_X is defined as the union of two Poincaré sections P_{X_+} and P_{X_-} defined as follows:

$$P_{X_+} = \{(X, Y) \in \mathbb{R}^2 | X = X_F, \dot{X} < 0\} \tag{32}$$

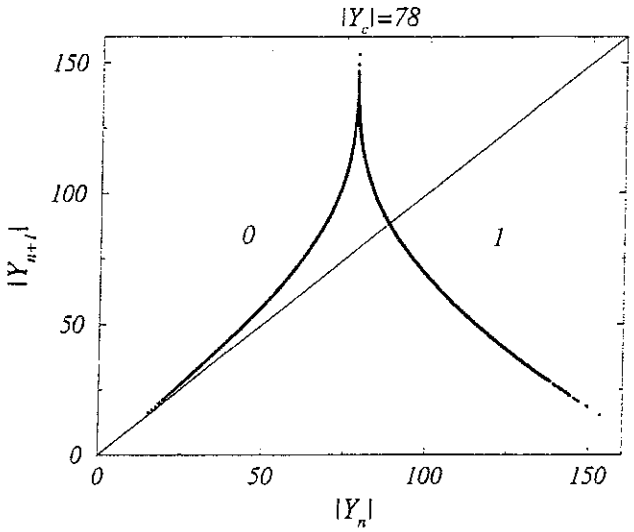

Fig. 17. First-return map to the Poincaré set P_X computed with the invariant variable $|Y|$.

and

$$P_{X_-} = \{(X, Y) \in \mathbb{R}^2 | X = -X_F, \dot{X} > 0\} \tag{33}$$

where $X_F = \sqrt{b(R-1)}$. In other words, the Poincaré set is constituted by the union of the Poincaré section P_{X+} computed in the fundamental domain $\mathcal{D}$ and of the Poincaré section P_{X-}, symmetrical with respect to P_{X+}, computed in the copy $\gamma\mathcal{D}$ of the fundamental domain, i.e. we have a Poincaré section in each wing.

The first-return map (Fig. 17) is computed with an invariant variable which may be taken as the absolute value of the Y-coordinate. This invariant variable mods out the equivariant nature of the Y-variable and consequently projects the dynamics on the fundamental domain $\mathcal{D}$.

A map similar to the Lorenz map [Lorenz, 1963] is then obtained exhibiting a critical point which is located at $Y_c = 78$. As on the original attractor, the increasing branch, labeled 0, is associated with the evolution of the trajectory in the same wing and the decreasing branch, labeled 1, with the transition from one wing to the other. The deep difference with the original attractor is that local torsions of band 1 are opposite, $+\pi$ on $\mathcal{D}$ and $-\pi$ on $\gamma\mathcal{D}$ [Fig. 19(a)].

In [Letellier *et al.*, 1994], we presented the topological procedure to characterize an attractor in the case where the symmetry preserves the rotation sign but this condition is not met in the case of an inversion symmetry [Letellier & Gouesbet,

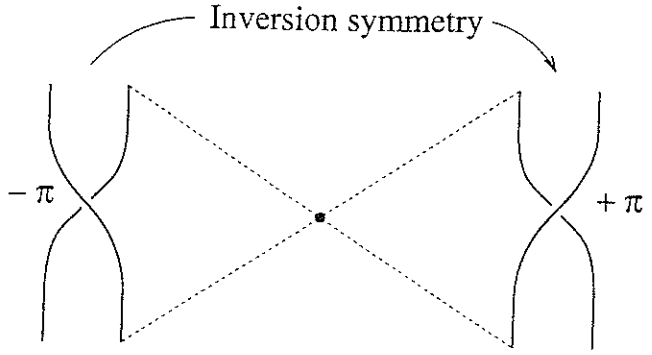

Fig. 18. Rotation sign is reversed under an inversion symmetry.

1996]. Actually an inversion symmetry reverses the rotation sign (Fig. 18). This property will have deep consequences on the fundamental linking numbers $\mathcal{L}(N_i, N_j)$ as described below.

From the mask of A_x [Fig. 19(a)], we extract the mask associated with the fundamental domain $\mathcal{D}$ and its copy $\gamma\mathcal{D}$, respectively Fig. 19(b). Let us insist on the fact that Fig. 19(b) presents both $\mathcal{D}$ and $\gamma\mathcal{D}$, i.e. it exhibits two fundamental domains in so far as either $\mathcal{D}$ or $\gamma\mathcal{D}$ could be chosen as the fundamental domain, this choice being arbitrary. Two fundamental templates are then proposed [Fig. 19(c)]. One may remark that the

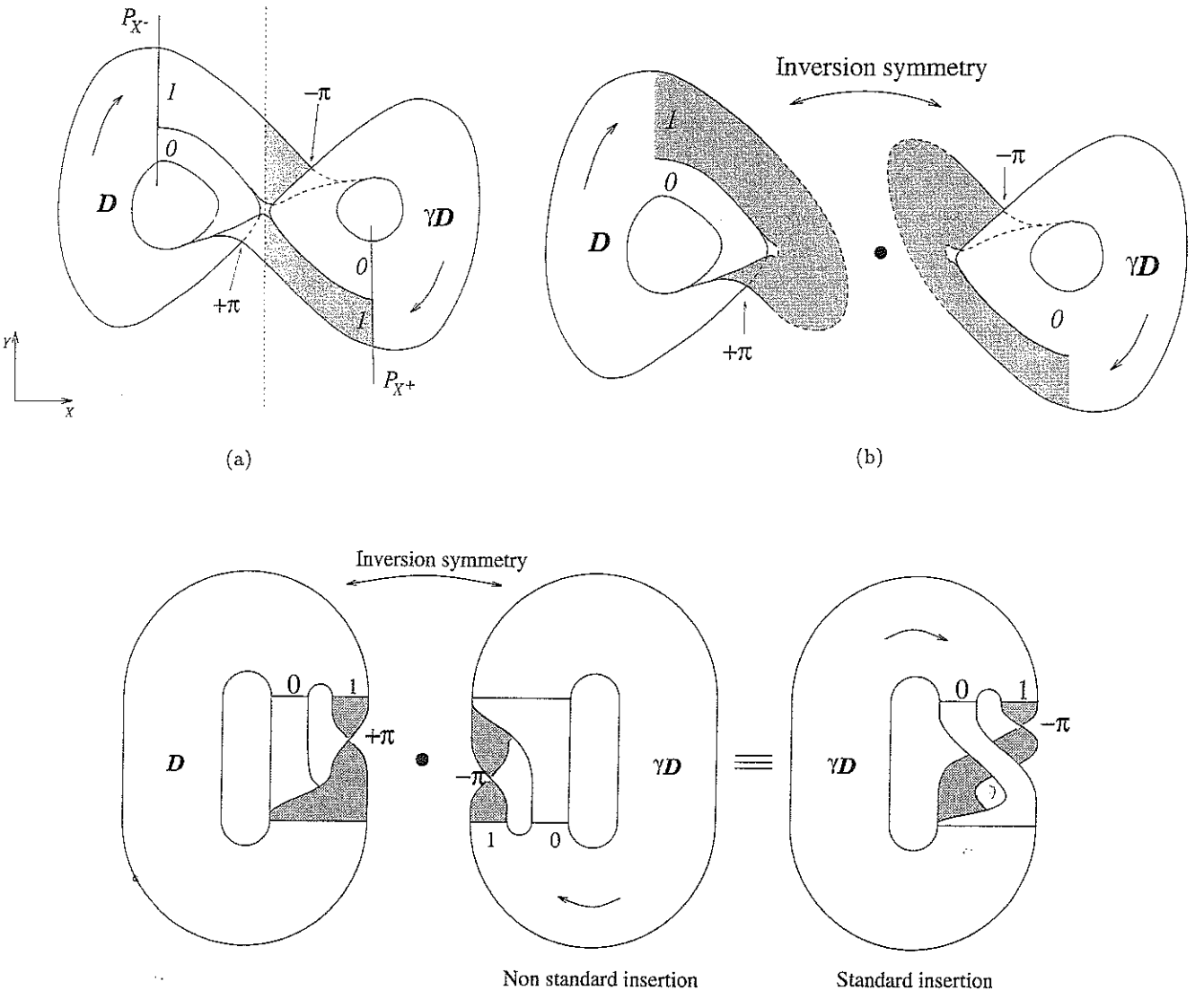

Fig. 19. Extraction of the template from the mask of the z-induced template. (a) Equivariant mask of A_x: the fundamental domain $\mathcal{D}$ and its copy $\gamma\mathcal{D}$ are bounded by the dashed line. The Poincaré sections P_X are also displayed. (b) Schematic view of the masks associated with $\mathcal{D}$ and $\gamma\mathcal{D}$ of A_x. (c) Templates of the fundamental domain $\mathcal{D}$ and of its copy $\gamma\mathcal{D}$.

fundamental template associated with the fundamental domain $\mathcal{D}$ presents a band 1 with a positive π-twist while the template associated with its copy $\gamma\mathcal{D}$ has a band 1 with a negative π-twist: this is a consequence of the inversion symmetry which reverses the rotation sign in contrast with the previously discussed case of axial symmetry. Then, using the standard insertion convention, the templates are described by the linking matrices

$$M_{\mathcal{D}} = \begin{pmatrix} 0 & 0 \\ 0 & +1 \end{pmatrix} \quad \text{and} \quad M_{\gamma\mathcal{D}} = \begin{pmatrix} 0 & -1 \\ -1 & -1 \end{pmatrix}, \tag{34}$$

respectively. One may remark that the template of the fundamental domain is the same as for the fundamental domain of the original attractor. Consequently, if we mod out the symmetry, the template of the reconstructed attractor induced by the x-time series is the same as for the original Lorenz system. So the two different dynamical systems have a fundamental domain exhibiting the same structure (horseshoe dynamics).

As both fundamental templates topologically characterize the attractor (in the restricted sense), we cannot unambiguously determine the sign of the local torsion of band 1. Indeed, the choice of the fundamental domain $\mathcal{D}$ is arbitrary (the right wing could be also chosen as the fundamental domain). Therefore, the sign of the fundamental linking number $\mathcal{L}(N_i, N_j)$ is arbitrary too. For these reasons, we prefer to introduce an unsigned fundamental linking number $\tilde{\mathcal{L}}(N_i, N_j)$. Let us note that the introduction of unsigned fundamental linking numbers is deeply related to the fact that restricted topological equivalence is not topological equivalence *stricto sensu*. Indeed, topological equivalence *stricto sensu* requires the use of signed linking numbers [Letellier & Gouesbet, 1996].

We now emphasize the usefulness of working with such a fundamental domain (at least in the present case of inversion symmetry). Due to the inversion symmetry which reverses the rotation sign, a signed crossing on a wing of A_x is opposite to its corresponding crossing (under the action of γ) on the other wing. Thus linking numbers $L(N_i, N_j)$ between two symmetric orbits are always equal to 0. Then topological equivalence *stricto sensu* does not sufficiently discriminate the different dynamics associated with symmetrical orbits. Topological characterization should therefore preferably be performed by considering a fundamental domain and a fundamental linking number.

Thus, as signed crossings are reversed under the action of γ, we have to work independently on the fundamental domain $\mathcal{D}$ (left wing) and on its copy $\gamma\mathcal{D}$ (right wing). The fundamental domain and its copy are easily generated on an XY-plane projection by drawing a dashed line defined by $X = 0$ [Fig. 19(a)]. One may check on Fig. 19(a) that an oriented crossing in $\mathcal{D}$ is mapped to an opposite crossing in $\gamma\mathcal{D}$ under the action of the γ-matrix. Signed crossings are then counted independently on $\mathcal{D}$ and $\gamma\mathcal{D}$ and the unsigned fundamental linking number $\tilde{\mathcal{L}}(N_i, N_j)$ is given by:

$$\tilde{\mathcal{L}}(N_i, N_j) = \frac{1}{2}\left[\frac{1}{2}\left|\sum_{p_1}\epsilon(p_1)\right| + \frac{1}{2}\left|\sum_{p_2}\epsilon(p_2)\right|\right] \tag{35}$$

in which p_1 designates a crossing between N_i and N_j on the fundamental domain $\mathcal{D}$ and p_2 a crossing between N_i and N_j on its copy $\gamma\mathcal{D}$. Such an unsigned fundamental linking number allows the provision of an invariant integer which is predicted by the fundamental template modulo the sign. It acts in a way similar to the fundamental linking number introduced in Sec. 3.2.2.

Indeed, due to the equivariance properties, to each oriented crossing between an orbit N_i and an orbit N_j on the fundamental domain is associated an oriented crossing on its copy but, as the inversion symmetry reverses the rotation sign, a positive (negative) crossing in $\mathcal{D}$ is found negative (positive) on $\gamma\mathcal{D}$. On the x-induced attractor, all the positive (negative) crossings counted on $\mathcal{D}$ are counted as negative (positive) on $\gamma\mathcal{D}$. If one only takes into account the oriented crossings on $\mathcal{D}$, the half-sum of these is found to be equal to the linking number predicted by the fundamental domain. Conversely, when the copy $\gamma\mathcal{D}$ is considered, the half-sum is found to be the opposite of the linking number predicted by the fundamental template. Nevertheless, the relative organization of the periodic orbits is found to be the same on $\mathcal{D}$ and $\gamma\mathcal{D}$ if we mod out the rotation sign as required in the presence of an inversion symmetry.

For instance, let us determine the fundamental linking number between two couples of periodic orbits encoded by (101, 10) and (100, 1), respectively. The unsigned fundamental linking number $\tilde{\mathcal{L}}(101, 10)$ is then found to be equal to 2 (Fig. 20) which is therefore equal (within the value of the sign) to the fundamental linking number $\mathcal{L}(101, 10)$ obtained on the original Lorenz attractor [Letellier & Gouesbet, 1996]. The unsigned

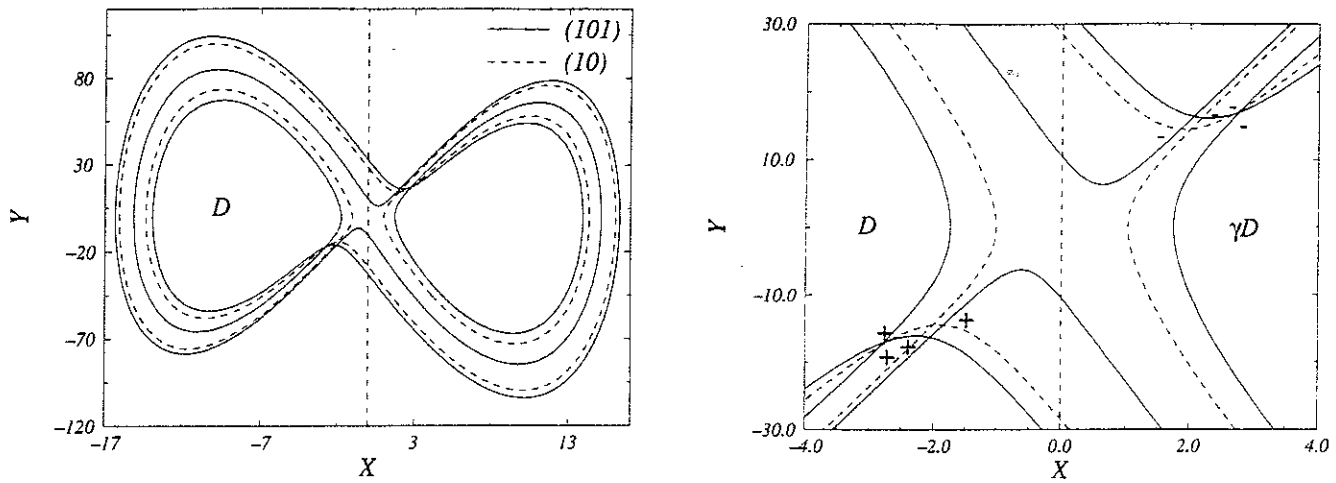

Fig. 20. Plane projection of the orbit pair (101, 10): $\tilde{\mathcal{L}}(101, 10) = \frac{1}{4}(|+4| + |-4|) = 2$. (a) Orbit couple (101, 10). (b) Blow up.

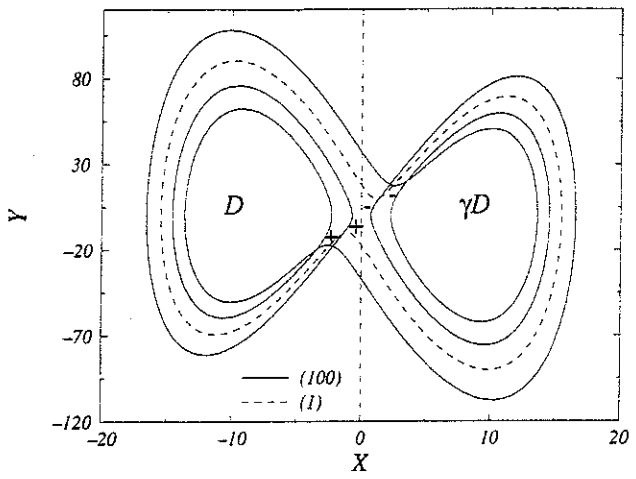

Fig. 21. Plane projection of the orbit pair (100, 1): $\tilde{\mathcal{L}}(100, 1) = \frac{1}{4}(|+2| + |-2|) = 1$.

fundamental linking number is then also in agreement with the template construction. Similarly, the unsigned fundamental linking number $\tilde{\mathcal{L}}(100, 1)$ is found to be equal to 1 (Fig. 21) and may be easily checked by a construction on the original template.

Topological properties are here checked in the weak sense (restricted topological equivalence); in particular, information about the rotation sign remains unavailable.

3.2.3. *Topological analysis of the symmetric attractor*

We have seen in Sec. 3.2.2. that the dynamical behavior of an equivariant system is conveniently analyzed by working in a fundamental domain, requiring the use of a Poincaré set instead of a Poincaré section. In the case of the symmetric attractor generated by the electronic circuit, such a Poincaré set P_{EC} is defined as the union of two Poincaré sections P_{X_+} and P_{X_-} which are defined by

$$P_{X_+} = \{(V, W) \in \mathbb{R}^2 | U = 4.0, \dot{U} < 0\} \qquad (36)$$

and

$$P_{X_-} = \{(V, W) \in \mathbb{R}^2 | U = -4.0, \dot{U} > 0\} \qquad (37)$$

The first-return map is then computed with an invariant variable taken as

$$\tilde{V} = \begin{cases} V & \text{if } U = 4.0 \\ -V & \text{if } U = -4.0 \end{cases} \qquad (38)$$

The first-return map is displayed in Fig. 22.

One may then remark that a small departure from the symmetry is exhibited by the first-return map since the points associated with the fundamental domain $\mathcal{D}$ define a curve which is slightly different from the one constituted by the points associated with the copy $\gamma\mathcal{D}$ of the fundamental domain. This slight difference may come from a small residual defect in the experimental set-up. Indeed, the nonlinearity in real circuit cannot be made perfectly symmetric.

Nevertheless, in order to perform a pertinent topological analysis, we had better eliminate this departure from symmetry. This may be achieved

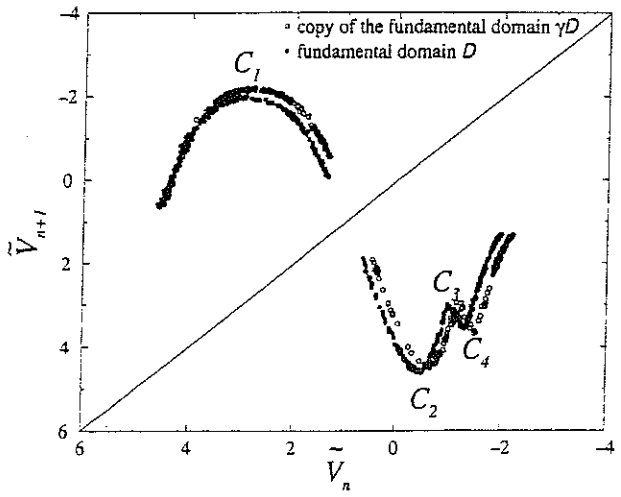

Fig. 22. First-return map to the Poincaré set P_{EC} computed with the invariant variable $\tilde{V}$.

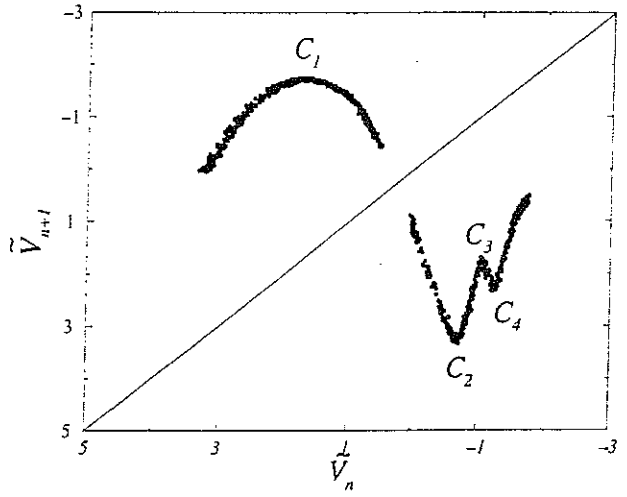

Fig. 23. First-return map to the Poincaré set computed with the new definition of the invariant variable $\tilde{V}$.

rather well by redefining the invariant variable $\tilde{V}$ as

$$\tilde{V} = \begin{cases} V & \text{if } U = 4.0 \\ -V + 0.18 & \text{if } U = -4.0 \end{cases} \tag{39}$$

The first-return map computed with this new definition of the invariant variable is displayed in Fig. 23. It now approximates well enough a one-dimensional map and exhibits five monotonic branches separated by four critical points which read as:

$$\begin{cases} C_1 = 1.70 \\ C_2 = -0.66 \\ C_3 = -1.05 \\ C_4 = -1.23 \end{cases} \tag{40}$$

Despite the fact that for our purposes this approximation is valid, one has to understand that the use of this approximation is limited. Indeed, it has been shown in previous studies of the circuit that the symmetric chaotic attractor is associated with the bifurcations of homoclinic orbits. These homoclinic orbits are formed by the one-dimensional unstable manifold of the saddle-focus located in the origin of the phase space. For the parameters of the circuit which correspond to the regime of symmetric chaotic oscillations, this saddle-focus is characterized by positive saddle-focus value $\Sigma_{sf} = \lambda_1 + Re\lambda_{2,3}$, where λ_1 and $\lambda_{2,3}$ are real and complex-conjugate eigenvalues of the saddle-focus. The dynamics of the systems with a homoclinic orbit originated from a saddle-focus was theoretically studied in a series of papers [Shilnikov, 1970; Belyakov, 1984]. The results of this theory indicate that the flow of the trajectories which passes through the vicinity of the saddle-focus has a twisted structure. In the case of positive saddle-focus value, this twisted structure will provide multiple folding of the shape of the first-return map. These foldings asymptotically merge to the point which is the image of the one-dimensional manifold of the saddle-focus [Glendining & Sparrow, 1991]. Therefore, the first-return map computed from the data contains multiple foldings in a narrow region located between the points C_2 and C_3. The influence of this region on the topology of the symmetric attractor can be very important. However, the noise in the experimental setup and the limitations of using a one-dimensional approximation of the map do not allow us to describe this region in detail. Therefore, the use of the approximated map which contains a small number of the foldings is valid only for the trajectories which are out of this narrow region.

The population of periodic orbits is now extracted from the Poincaré set P_{EC} and encoded by using:

$$\begin{cases} 0 & \text{if} \quad \tilde{V}_n < C_1 \\ 1 & \text{if} \quad C_1 < \tilde{V}_n < C_2 \\ 2 & \text{if} \quad C_2 < \tilde{V}_n < C_3 \\ 3 & \text{if} \quad C_3 < \tilde{V}_n < C_4 \\ 4 & \text{if} \quad C_4 < \tilde{V}_n \end{cases} \tag{41}$$

The orbit spectrum is reported in Table 4. As is easily viewed on the first-return map (Fig. 23), no period-1 orbit is found within the attractor since the map does not cross the bissectrix line.

Table 4. Population of periodic orbits embedded within the symmetric attractor for $\alpha = 18.9$.

Period	(W)	Period	(W)
2	10		414040
	20		413041
	30		412041
	40		412040
	41		412030
4	2120		412020
	3020		412010
	4140		412011
	4130		411011
	4121		411010
	4120		411020
6	201020		411030
	201011		411040
	414041		

As for any symmetric system, there exist two kinds of periodic orbits. The first kind is constituted by asymmetric orbits which appear by pairs [Fig. 24(a)]. The second kind is constituted by symmetric orbits which describe twice their symbolic sequence before returning to their initial conditions [Fig. 24(b)].

A mask is now extracted from the attractor displayed in Fig. 16. Nevertheless, due to the number of stripes and the structure of the attractor, a clear sketch of this mask cannot be conveniently given in this paper. The fundamental template which synthetizes the topology of the fundamental domain $\mathcal{D}$ is given in Fig. 25. Its linking matrix reads as:

$$M_{\mathcal{D}} \equiv \begin{pmatrix} 0 & 0 & 0 & 0 & 0 \\ 0 & +1 & +1 & +1 & +1 \\ 0 & +1 & +2 & +1 & +2 \\ 0 & +1 & +1 & +3 & +2 \\ 0 & +1 & +2 & +2 & +2 \end{pmatrix} \tag{42}$$

This linking matrix is given for the fundamental domain $\mathcal{D}$ which is taken as indicated in Fig. 16.

But let us recall that an inversion symmetry reverses the signs of rotation. Consequently, the fundamental template associated with the copy of the fundamental domain is defined by a linking matrix which reads as:

$$M_{\gamma\mathcal{D}} \equiv \begin{pmatrix} 0 & -1 & -1 & -1 & -1 \\ -1 & -1 & -2 & -2 & -2 \\ -1 & -2 & -2 & -2 & -3 \\ -1 & -2 & -2 & -3 & -3 \\ -1 & -2 & -3 & -3 & -2 \end{pmatrix} \tag{43}$$

Due to the standard insertion convention [Melvin & Tufillaro, 1991], this linking matrix is not the opposite of $M_{\mathcal{D}}$. Nevertheless, the fundamental template which is associated with the copy of the fundamental domain is able to predict fundamental linking numbers counted on $\gamma\mathcal{D}$. Furthermore, by working

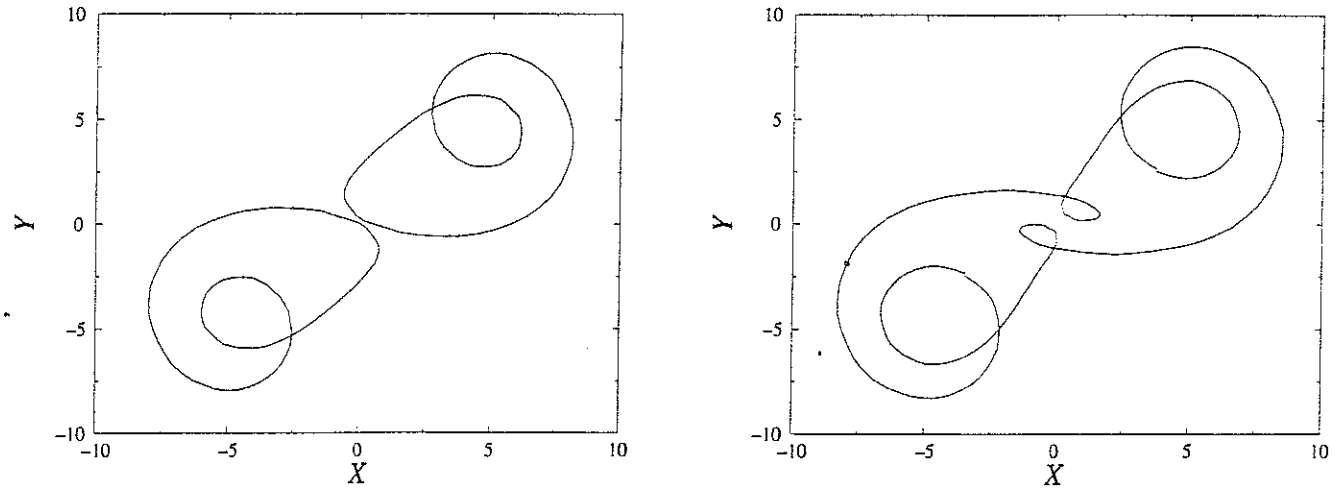

Fig. 24. The two kinds of periodic orbits. (a) Pair of asymmetric orbits encoded by (10). (b) Symmetric orbit encoded by (30).

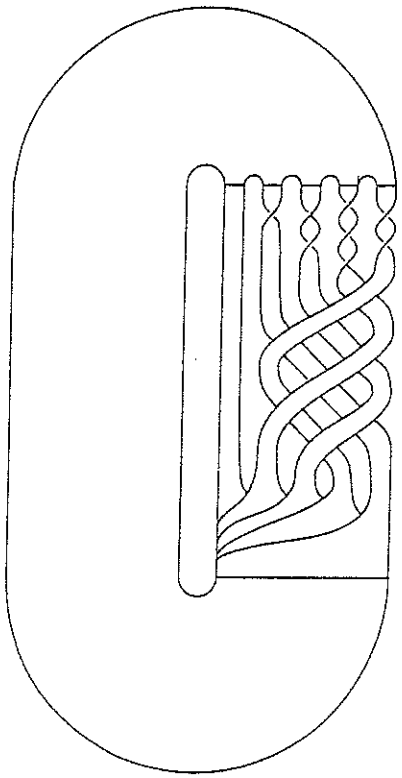

Fig. 25. Template of the fundamental domain of the symmetric attractor.

with unsigned linking numbers, the two linking matrices may be simultaneously checked with plane projections of orbit couples. For instance, the unsigned fundamental linking numbers $\tilde{\mathcal{L}}(40, 30)$ and $\tilde{\mathcal{L}}(30, 10)$ are found to be equal to 2 from the template in agreement with the plane projections (Fig. 26).

The reader may check that the linking matrix $M_{\gamma\mathcal{D}}$ is consistent with the linking matrix M_S of the attractor A^+, i.e. the third first lines and columns are identical to the associated lines and columns of M_S.

4. The Models

4.1. *Chua's circuit*

The main objective of this section is to construct templates for two members of a family of chaotic attractors called Chua's attractors: the spiral type and the double scroll attractors, which have been the object of a couple of recent papers by Kocarev *et al.* [1994a, 1994b]. The motivation for studying Chua's circuit is that it is a model of an electronic circuit whose attractors look rather similar to the ones observed on the electronic circuit described in the previous sections. By using the topological characterization, we would like to determine if an equivalence exists between the previously discussed experimental circuit and the simple autonomous physical system proposed by Chua [1992].

4.1.1. *The system*

Chua's system to model the dynamics of Chua's circuit is constituted by a set of three ordinary

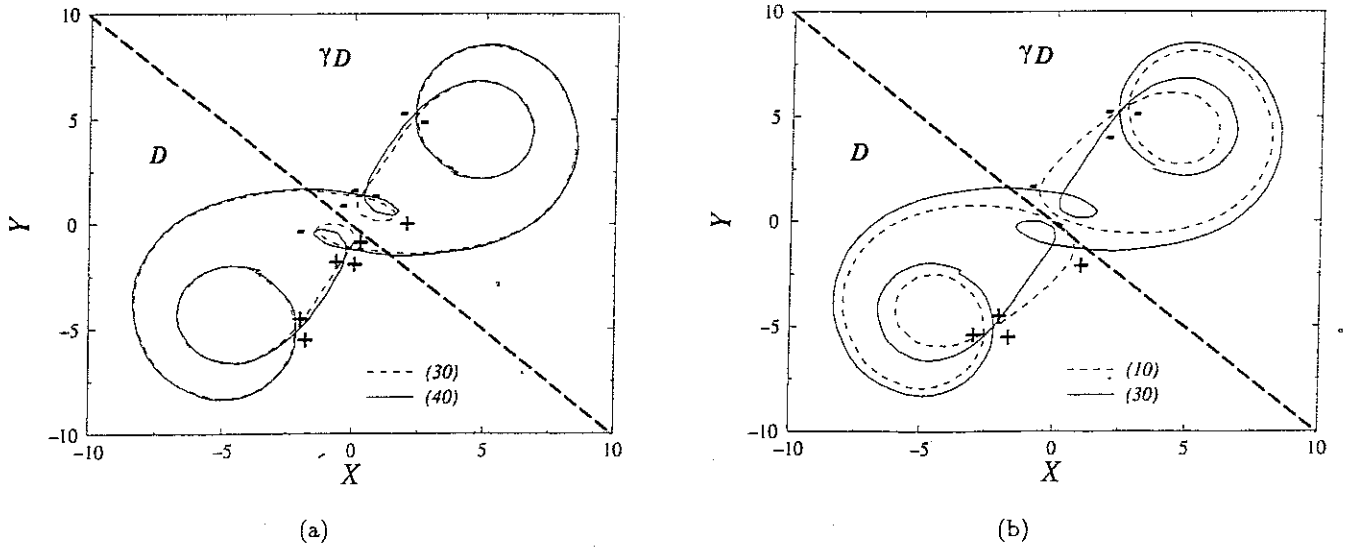

Fig. 26. Plane projections of two couples of periodic orbits. (a) $\mathcal{L}(40,30) = \frac{1}{2}(\frac{1}{2}|+5-1|+\frac{1}{2}|-5+1|) = 2$. (b) $\mathcal{L}(30,10) = \frac{1}{2}(\frac{1}{2}|+4|+\frac{1}{2}|-4|) = 2$.

differential equations which read as:

$$\begin{cases} \dot{x} = \alpha\,[y - x - h(x)] \\ \dot{y} = x - y + z \\ \dot{z} = -\beta y \end{cases} \tag{44}$$

where

$$h(x) = m_1 x + \frac{(m_0 - m_1)}{2}\,[|x+1| - |x-1|] \tag{45}$$

The control parameters of the system are fixed as $\beta = 100/7$, $m_0 = -8/7$, $m_1 = -5/7$, while α is a variable control parameter. The vector field defined by these equations is equivariant under a matrix which reads as

$$\gamma_c = \begin{pmatrix} -1 & 0 & 0 \\ 0 & -1 & 0 \\ 0 & 0 & -1 \end{pmatrix} \tag{46}$$

This matrix defines an inversion symmetry. If $8.45 < \alpha < \alpha_c = 8.80642$, there exist two symmetrical attractors each with its own basin of attraction. For α_c, a boundary crisis occurs and a larger symmetric attractor, resulting from the merging of the two attractors A^- and A^+, is created. This evolution is similar to the one observed on the experimental circuit and on the model studied in the previous section.

In order to gain a precise comparison between Chua's model and the behavior of the experimental electronic circuit, we will use the topological characterization. Actually, a description of the topology of this model has already been performed by Kocarev *et al.* [1994a, 1994b] without, however, taking into account the equivariance of the vector field defined by Eq. (44). Here, in contrast, we will give a topological analysis of the system for $\alpha = 8.8$ and $\alpha = 9.0$, generating attractors which look similar to the ones of the experimental circuit and which account for the equivariance properties.

4.1.2. *The pair of simple attractors*

For $\alpha = 8.8$, the asymptotic motion settles down on to one of two chaotic attractors depending on the initial conditions. One of these two attractors is displayed in Fig. 27.

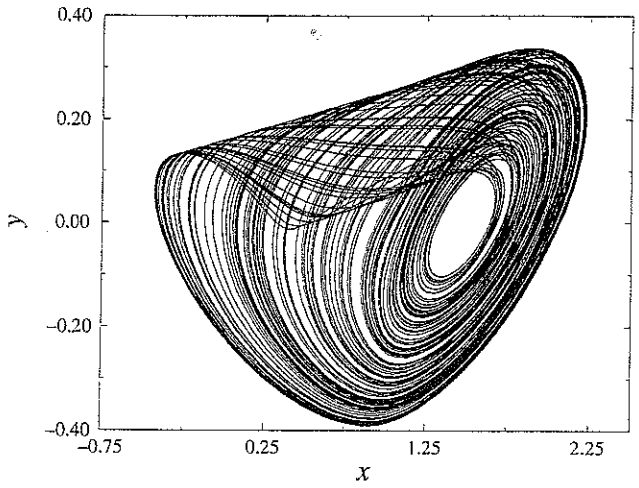

Fig. 27. One of the two attractors which are symmetrical one with respect to the other.

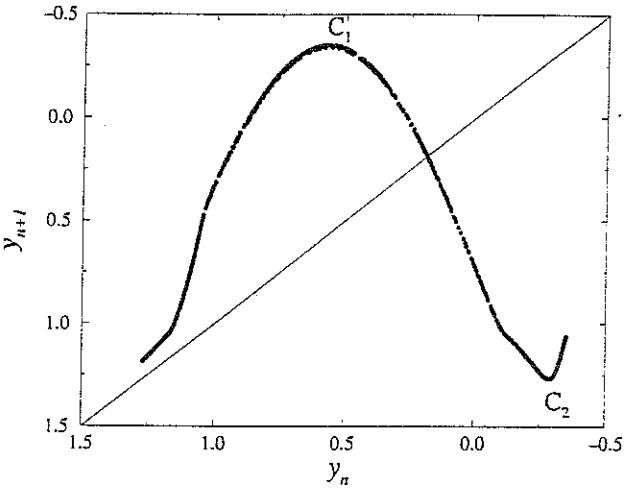

Fig. 28. First-return map to the Poincaré section P_c.

This attractor is studied via the Poincaré section P_c defined as:

$$P_c = \{(x, z) \in \mathbb{R}^2 | y = -0.05,\ \dot{y} > 0\} \tag{47}$$

From this Poincaré section, a first-return map is computed with the x-coordinate (Fig. 28). Three monotonic branches are exhibited and separated by two critical points which read as:

$$\begin{cases} C_1 = 0.572 \\ C_2 = -0.288 \end{cases} \tag{48}$$

Periodic orbits are extracted and encoded by using:

$$\begin{cases} 0 & \text{if} \quad C_1 < y_n \\ 1 & \text{if} \quad C_2 < y_n < C_1 \\ 2 & \text{if} \quad y_n < C_2\,. \end{cases} \tag{49}$$

Table 5. Population of periodic orbits embedded within the simple attractor for $\alpha = 8.8$.

sequence	sequence	sequence	sequence
1	1011	10100	20000
10	1001	10111	20001
101	1000	10110	20011
100	2000	10001	20010
200	2001	10000	

The orbit spectrum is reported in Table 5.

The symbolic plane is computed and the kneading forward coordinates associated with the critical points C_1 and C_2 are

$$\begin{cases} \alpha_1 = 0.5079 \\ \alpha_2 = 0.0020 \end{cases} \tag{50}$$

respectively. The associated kneading sequences are written as

$$\begin{cases} K_1 = (\overline{200}) \\ K_2 = (\overline{000\bar{1}}) . \end{cases} \tag{51}$$

All periodic orbits extracted from the attractors are allowed by the kneading sequences except the period-3 orbit encod by (201) which is created by a saddle-node bifurcation, implying also the orbit (200). This orbit is already well approximated by a part of the chaotic trajectory although it is not really created.

By computing linking numbers between a few couples of low period orbits, we found that linking numbers are well predicted by the template defined by the linking matrix (15) without any discrepancy. See for instance the plane projection of orbits encoded by (201) and (1) displayed in Fig. 29.

The attractor generated by Chua's circuit is therefore topologically equivalent to the one generated by the experimental electronic circuit. The orbit spectra are however different. They could be adjusted by acting on the control parameters α and β.

4.1.3. *The double scroll attractor*

For $\alpha = 9.0$, after the boundary crisis, the asymptotic motion settles down on to a double scroll attractor which is displayed in Fig. 30.

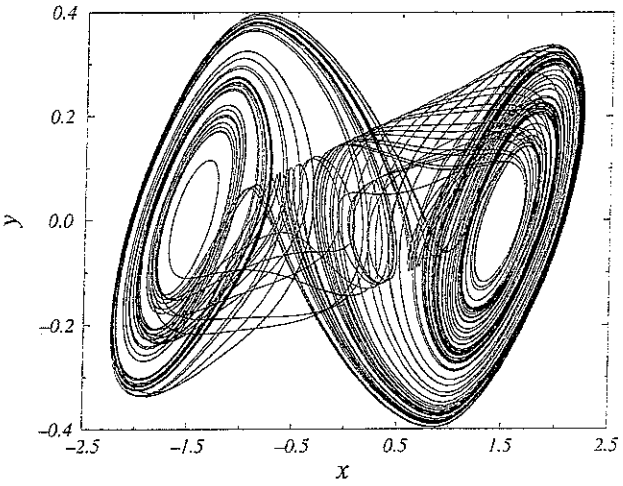

Fig. 30. The double scroll attractor for $\alpha = 9.0$.

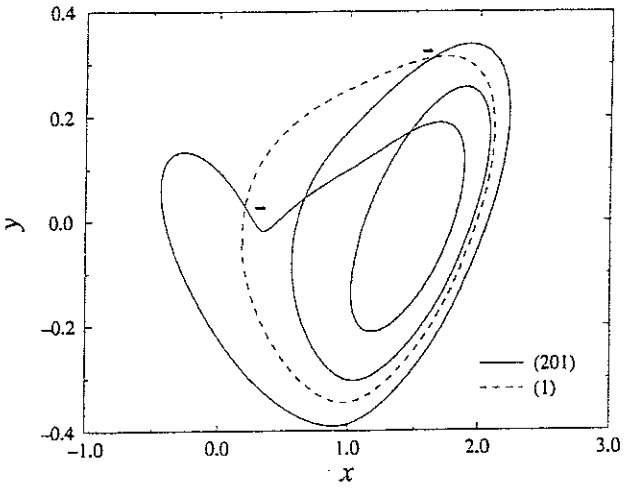

Fig. 29. Plane projection of periodic orbits encoded by (201) and (1). The linking number $L(201, 1)$ is equal to $\frac{1}{2}(-2) = -1$ as on the experimental circuit (see Fig. 8).

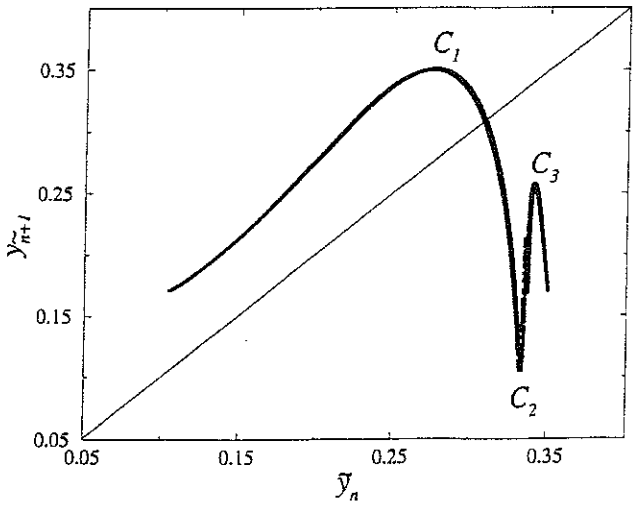

Fig. 31. First-return map to the Poincaré set P_S built on the $|y|$ invariant coordinate.

This attractor is studied via a Poincaré set P_S defined as the union of two Poincaré sections reading as:

$$P_{S^+} = \{(y, z) \in \mathbb{R}^2 | x = 1.25, \dot{x} < 0\} \tag{52}$$

and

$$P_{S^-} = \{(y, z) \in \mathbb{R}^2 | x = -1.25, \dot{x} > 0\}. \tag{53}$$

A first-return map is computed by using the absolute value of the y-coordinate to obtain an invariant variable as required to perform the topological analysis in the fundamental domain $\mathcal{D}$. The map, displayed in Fig. 31, exhibits four monotonic branches separated by three critical points according to

$$\begin{cases} C_1 = 0.276 \\ C_2 = 0.333 \\ C_3 = 0.342\,. \end{cases} \tag{54}$$

The population of periodic orbits is extracted and encoded by using:

$$\begin{cases} 0 & \text{if} \quad |y_n| < C_1 \\ 1 & \text{if} \quad C_1 < |y_n| < C_2 \\ 2 & \text{if} \quad C_2 < |y_n| < C_3 \\ 3 & \text{if} \quad C_3 < |y_n|\,. \end{cases} \tag{55}$$

The orbit spectrum is reported in Table 6. As expected on a symmetric attractor, two kinds of periodic orbits are again found.

Once more, linking numbers counted on plane projections of orbit couples are found to be equal to the ones predicted by the template defined by the linking matrix (42). The double scroll attractor of the Chua's circuit is therefore topologically compatible with the one observed on the experimental circuit. A plane projection of orbits encoded by (30) and (10) is given as an example (Fig. 32).

Table 6. Population of periodic orbits embedded within the double scroll attractor for $\alpha = 9.0$.

sequence	sequence	sequence	sequence
10	4140	414040	412011
20	4130	413041	411011
30	4121	412041	411010
40	4120	412040	411020
41	201020	412030	411030
2120	201011	412020	411040
3020	414041	412010	

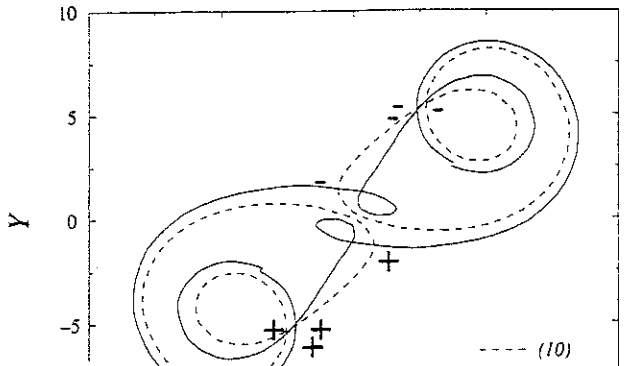

Fig. 32. Plane projection of periodic orbits encoded by (30) and (10). The linking number $L(30, 10)$ is equal to $\frac{1}{2}[\frac{1}{2}|+4|+\frac{1}{2}|-4|] = 2$.

4.2. *The second model*

Let us consider a model which describes the dynamics of this experimental circuit [Volkovski & Rulkov, 1988]. The model is constituted by a three variable system of differential equations which reads as:

$$\begin{cases} \dot{x} = y \\ \dot{y} = -x - \delta y + z \\ \dot{z} = \gamma\,[\alpha F(x) - z] - \sigma y \end{cases} \tag{56}$$

where x is the voltage across the capacitor C and $y = \sqrt{L/C'}\; i(t)$ with $i(t)$ the current through the inductor L. Also, z is the voltage across the capacitor C'. Time has been scaled as $\tau = t\sqrt{LC'}$. The parameters of this system have the following dependence on the physical values of the circuit elements:

$$\gamma = \frac{\sqrt{LC}}{RC'}, \quad \delta = r\sqrt{\frac{C}{L}}, \quad \sigma = \frac{C}{C'} \tag{57}$$

where the values of control parameters correspond to the experimental values of the circuit studied in Sec. 3. The nonlinearity $F(x)$ can be approximated by

$$F(x) = \begin{cases} 0.528 & \text{for} \quad x < -1.2 \\ x(1 - x^2) & \text{for} \quad -1.2 < x < -1.2 \\ -0.528 & \text{for} \quad 1.2 < x\,. \end{cases} \tag{58}$$

The model has the nice feature of being linear in the neighborhood of the origin. The development of the trajectory is bounded when x exceeds threshold. The trajectories are then reinjected at the upper level while maintaining symmetry. The vector field so defined is equivariant with an equivariance matrix reading as:

$$\gamma = \begin{pmatrix} -1 & 0 & 0 \\ 0 & -1 & 0 \\ 0 & 0 & -1 \end{pmatrix} \tag{59}$$

which again defines an inversion symmetry. Depending on the values of the control parameters, the behavior of the circuit settles down to a single symmetric attractor or to an asymmetric pair of attractors (one or the other attractor in the pair is reached depending on the initial conditions). Projections of these attractors are given in Figs. 33 and 34. The behavior of this model is therefore similar to that of Chua's circuit.

We will study the symmetric attractor for $\alpha = 15.8$ (note that an exact correspondence between the experimental and the model α-values does not exist). The attractor is symmetric and consequently must be characterized with the procedure required for systems with equivariance properties. A Poincaré set P_D is defined as the union of two Poincaré sections P_{D+} and P_{D-} which read as:

$$P_{D+} = \{(|y|, |z|) \in \mathbb{R}^2 | x = 0.8, \dot{x} < 0\} \tag{60}$$

and

$$P_{D-} = \{(|y|, |z|) \in \mathbb{R}^2 | x = -0.8, \dot{x} > 0\} \tag{61}$$

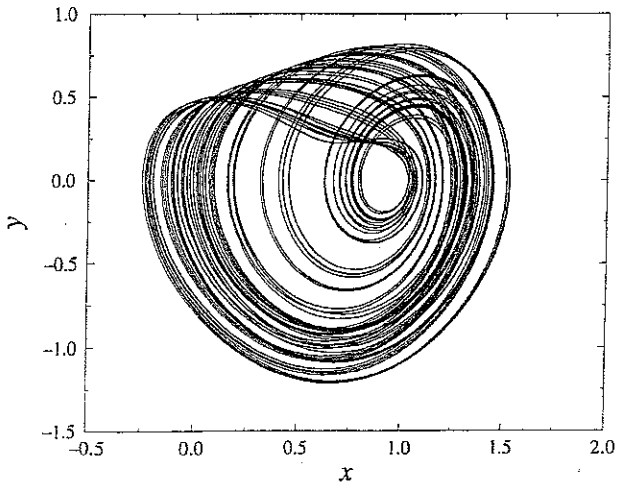

Fig. 33. One of the pair of attractors for $\alpha = 13.5$.

where the absolute values of y and z are required to work with invariant variables which project the dynamics on the fundamental domain. A first-return map is built with an invariant variable given by

$$w_n = |y_n| \cos\phi + |z_n| \sin\phi \tag{62}$$

where $\phi = \pi/6$ allowing the reduction of the layered structure which is present on the first-return maps built with $|y_n|$ or $|z_n|$. The first-return map so obtained is displayed in Fig. 35.

Four branches are essentially exhibited on the first-return map. In fact, there also exist two critical points between C_3 and C_4, but the corresponding branches are not sufficiently developed to be safely

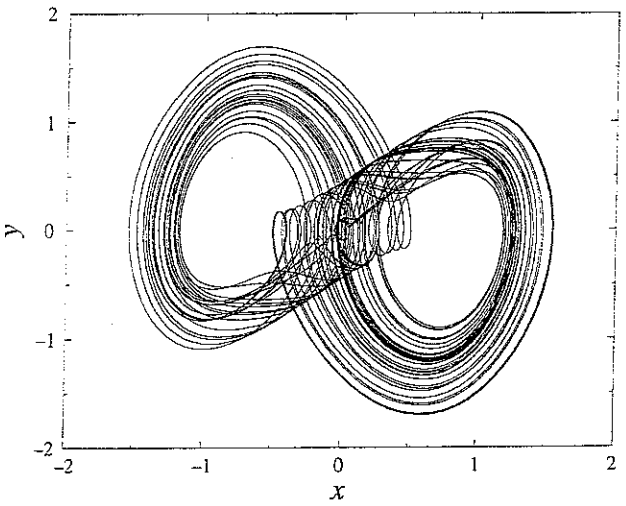

Fig. 34. The symmetric attractor for $\alpha = 15.8$.

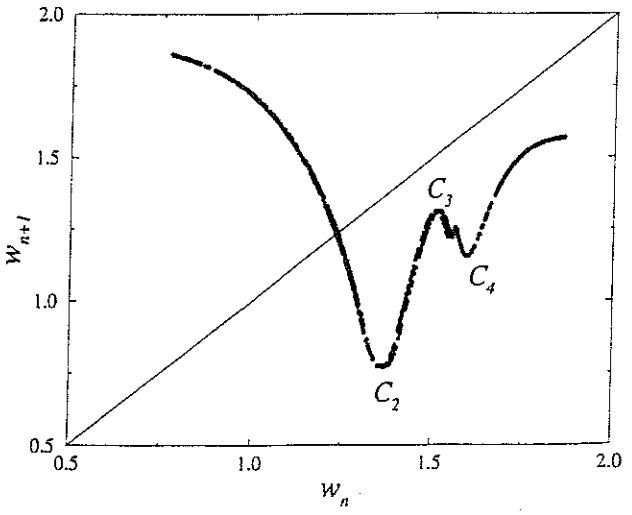

Fig. 35. First-return map to the Poincaré set P_D built with the invariant variable w_n.

taken into account in the symbolic dynamics of low periodic orbits. Consequently, only three critical points are taken into account as

$$\begin{cases} C_2 = 1.36 \\ C_3 = 1.51 \\ C_4 = 1.60\,. \end{cases} \tag{63}$$

One may remark that the first increasing branch encoded by 0 is not present on this attractor, i.e. stripe 0 is not visited by the asymptotic chaotic trajectory. The population of periodic orbits is extracted from the attractor and encoded by using:

$$K(w_n) = \begin{cases} 1 & \text{if} \quad w_n < C_2 \\ 2 & \text{if} \quad C_2 < w_n < C_3 \\ 3 & \text{if} \quad C_3 < w_n < C_4 \\ 4 & \text{if} \quad C_4 < w_n\,. \end{cases} \tag{64}$$

The model has now to be validated by using the topological analysis. This is achieved by comparing the topology of the attractor obtained by integrating the model and the attractor induced by the experimental data. We have to check if the unsigned linking numbers counted on plane projections of orbit pairs are in agreement with the template prediction. For instance, the unsigned fundamental linking number $\tilde{\mathcal{L}}(21,\,1)$ is found to be equal to 1 on the plane projection displayed in Fig. 36 and consequently is equal to the one predicted by the linking matrices $M_{\mathcal{D}}$ or $M_{\gamma\mathcal{D}}$.

All investigated linking numbers have been found to be in agreement with the template predictions. The topology of the attractor generated by the model is therefore compatible with the template induced by the experimental symmetric attractor. The same orbit spectrum could be obtained by acting on the control parameters of the model.

5. Nature of the Equivalence

We have seen that the attractors generated by Chua's system are topologically equivalent to the ones observed on the experimental electronic circuit. In this case, we have a favorable situation where the symmetry properties may be preserved by a reconstruction method starting from a single equivariant variable with an embedding dimension equal to 3.

This is confirmed by using the z-variable to obtain a reconstructed attractor (Fig. 37). This reconstructed attractor may be favorably compared with the X-induced attractor displayed in Fig. 16.

If the z-induced Chua's attractor looks rather similar to the experimental attractor A_X, this is not necessarily the case for each variable of the Chua's system. Indeed, it has been shown that each variable may give a particular and different point of view of a system when it is used to reconstruct a phase space [Letellier & Gouesbet, 1996]. Thus, although the measured x-variable from the experimental electronic circuit is rather close to the

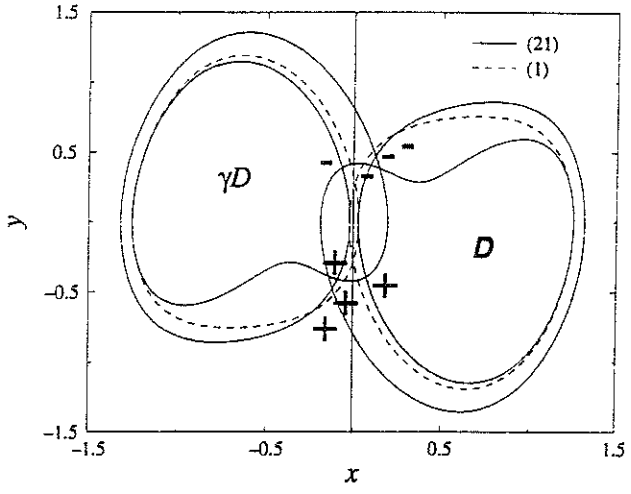

Fig. 36. Plane projection of orbits encoded by (21) and (1) extracted from the symmetric attractor. The unsigned fundamental linking number $\tilde{\mathcal{L}}(21,\,1)$ is found to be equal to 1.

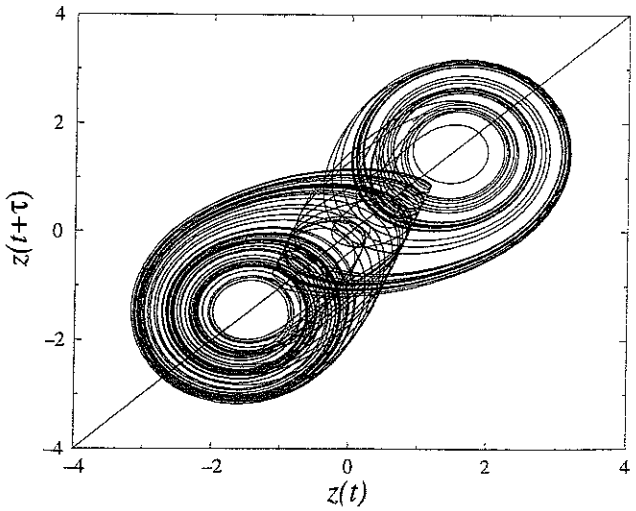

Fig. 37. z-induced attractor of the Chua's system. The three fixed points are located on the bissectrix line of the plane spanned by $\{z(t),\, z(t+\tau)\}$ where $\tau = 0.5s$.

z-variable of the Chua's circuit, it is not ensured that it remains true for the x- or y-variables.

In order to state the point taken in view of the variables, let us start by discussing the fixed points of Chua's equations. There are three fixed points. One, labeled F_0, is associated with the origin of the state space and the two others are given by:

$$F_\pm = \begin{cases} x_\pm = \pm\dfrac{3}{2} \\ y_\pm = 0 \\ z_\pm = \mp\dfrac{3}{2}. \end{cases} \tag{65}$$

The three fixed points are located on a line defined by $y = 0$ in the xy-plane. It then immediately appears that the y-variable provides a rather marginal view of the attractor since the three fixed points F_0 and $F_\pm$ are not distinguished by this variable. Consequently, the reconstructed attractor cannot exhibit three fixed points but only one. This result is easily viewed on the y-induced Chua's attractor displayed in Fig. 38.

Indeed, the y-induced attractor with a time delay reconstruction method (Fig. 38), although being equivariant, does not present two wings as exhibited on the original Chua's attractor. This is a great consequence of the absence of distinction between the three fixed points when using the y-variable. We have here an interesting case of a symmetric attractor reconstructed from an equivariant variable which does not exactly preserve the nature of the inversion symmetry of the original attractor. The two wings are now inextricably combined and it is even rather difficult to compute a pertinent Poincaré map.

When one uses a reconstruction method to obtain a global vector field, we generally possess a single scalar time series. Each variable spanning the reconstructed phase space is derived from a single one and therefore has the same point of view of the system. Therefore, when the dimension of the reconstructed phase space is small, the choice of the variable used for reconstruction is of importance.

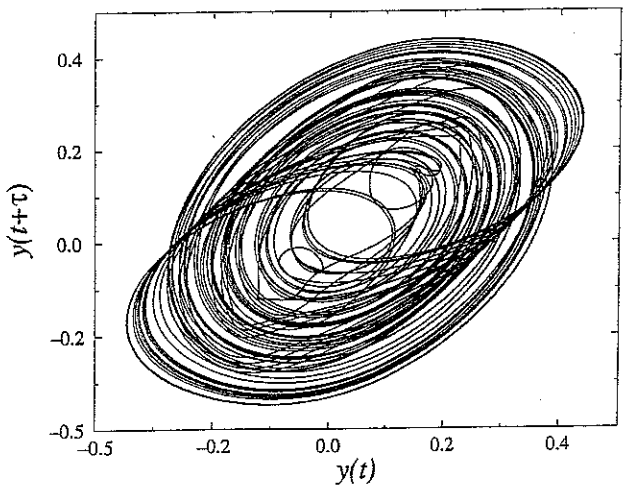

Fig. 38. y-induced attractor of the Chua's system. The time delay is $\tau = 0.4s$.

6. Conclusion

We have extensively studied an experimental electronic circuit for two control parameter values. We have shown that the dynamics presents some symmetry properties. The two experimental attractors have been found to be topologically compatible with two attractors of the Chua's circuit. Moreover, a model of the experimental circuit has been checked by using a topological analysis. We have also discussed the case when a variable may induce a topology modification. This is of particular interest for the choice of the recorded time series. Indeed, the second time series recorded on the experimental circuit has been found to induce an attractor whose topology is slightly different from the topology of the attractor induced by the first variable.

Acknowledgment

We wish to thank Reggie Brown (Institute for Nonlinear Science, University of California of San Diego, La Jolla, USA) for his helpful discussions.

References

Agarwal, A. K., Ahalpara, D. P., Kaw, P. K., Prablakera, H. R. & Sen, A. [1990] "Model equations from a chaotic time series," *J. of Phys.* **35**(3), 287–301.

Belyakov, L. [1984] "Bifurcation of the system with homoclinic curve of a saddle-focus with saddle quantity zero," *Math. Zam.* **36**, 838–843.

Breeden, J. L. & Hübler, A. [1990] "Reconstructing equations of motion from experimental data with hidden variables," *Phys. Rev.* **A42**(10), 5817–5826.

Brown, R., Rulkov, N. F. & Tracy, E. R. [1995] "Modeling and synchronizing chaotic systems from time-series data," *Phys. Rev.* **E49**(5), 3784–3800.

Casdagli, M., Eubank, S., Farmer, J. D. & Gibson, J. [1991] "State space reconstruction with noise," *Physica* **D51**, 52–98.

Chua, L. O. [1992] "The genesis of Chua's circuit," *Archiv fur Elektronic und Ubertragungstechnik* **46**, 250–257.

Crutchfield, J. P. & McNamara, B. S. [1987] "Equations of motion from a data series," *Complex Systems* **1**, 417–452.

Duan, B., Wang, Y. & Zhao, H. [1994] "Symbolic dynamics for the sin map," *Commun. Theor. Phys.* **22**, 299–306.

Dutertre, P. [1995] *Caractérization des attracteurs étranges par la population d'orbites périodiques* Ph'D dissertation, URA CNRS 230, LESP, Rouen, France.

Fa-Geng Xie. [1994] "Symbolic dynamics for the general quartic map," *Commun. Theor. Phys.* **22**, 43–52.

Fang, H. P. [1994] "Dynamics of strongly dissipative systems," *Phys. Rev.* **E49**(6), 5025–5031.

Farmer, J. D. & Sidorowitch, J. J. [1987] "Predicting chaotic time series," *Phys. Rev. Lett.* **59**, 845–848.

Fraser, A. M. & Swinney, H. L. [1986] "Independent coordinates for strange attractors from mutual information," *Phys. Rev.* **A33**(2), 1134–1140.

Gibson, J. F., Farmer, J. D., Casdagli, M. & Eubank, S. [1992] "An analytic approach to practical state space reconstruction," *Physica* **D57**, 1–30.

Giona, M., Lendini, F. & Cimagalli, V. [1991] "Functional reconstruction and local prediction of chaotic time series," *Phys. Rev.* **A44**(6), 3496–3502.

Glendining, P. & Sparrow, C. [1991] "Local and global behavior near homoclinc orbits," *J. Stat. Phys.* **35**, 645–696.

Gouesbet, G. & Maquet, J. [1992] "Construction of phenomenological models from numerical scalar time series," *Physica* **D58**, 202–215.

Gouesbet, G. & Letellier, C. [1994] "Global vector field reconstruction by using a multivariate polynomial L_2-approximation on nets," *Phys. Rev.* **E49**(6), 4955–4972.

Grassberger, P. & Proccacia, I. [1983] "Measuring the strangeness of strange attractors," *Physica* **D9**, 189–208.

Kennel, M. B., Brown, R. & Abarbanel, H. D. I. [1992] "Determining embedding dimension for phase-space reconstruction using a geometrical construction," *Phys. Rev.* **A45**, 3403–3411.

King, G. P. & Stewart, I. [1992] "Phase space reconstruction for symmetric dynamical systems," *Physica* **D58**, 216–228.

Kocarev, L., Tasev, Z., Dimovski, D. & Chua, L. O. [1994] "Knotted periodic orbits in Chua's circuit," *Int. J. Bifurcation Chaos* **4**(3), 609–621.

Kocarev, L., Tasev, Z. & Dimovski, D. [1994] "Topological description of a chaotic attractor with spiral structure," *Phys. Lett.* **A190**, 399–402.

Letellier, C., Dutertre, P. & Gouesbet, G. [1994] "Characterization of the Lorenz system taking into account the equivariance of the vector field," *Phys. Rev.* **E49**(4), 3492–3495.

Letellier, C., Le Sceller, L., Maréchal, E., Dutertre, P., Maheu, B., Gouesbet, G., Fei, Z. & Hudson, J. L. [1995] "Global vector field reconstruction from a chaotic experimental signal in copper electrodissolution," *Phys. Rev.* **E51**(5), 4262–4266.

Letellier, C., Le Sceller, L., Dutertre, P., Gouesbet, G., Fei, Z. & Hudson, J. L. [1995] "Topological characterization and global vector field reconstruction from experimental electrochemical system," *J. Phys. Chem.* **99**, 7016–7027.

Letellier, C., Dutertre, P., Reizner, J. & Gouesbet, G. [1996] "Evolution of a multimodal map induced by an equivariant vector field," *J. Phys* **A29**, 5359–5375.

Letellier, C. & Gouesbet, G. [1996] "Topological characterization of reconstructed attractors modeling out symmetries," *J. Phys. II* **6**, 1615–1638.

Lorenz, E. N. [1963] "Deterministic Nonperiodic Flow," *J. of the Atm. Sci.* **20**, 130–141.

Melvin, P. & Tufillaro, N. B. [1991] "Templates and framed braids," *Phys. Rev.* **A44** (6), 3419–3422.

Mindlin, G. B. & Solari, H. G. [1995] "Topologically inequivalent embeddings," *Phys. Rev.* **E52**(2), 1497–1502.

Packard, N. H., Crutchfield, J. P., Farmer, J. D. & Shaw, R. S. [1980] "Geometry from a time series," *Phys. Rev. Lett.* **45**(9), 712–716.

Palus, M. & Dvoràck, I. [1992] "Singular-value decomposition in attractor reconstruction. Pitfalls and precautions," *Physica* **D55**, 221–234.

Rulkov, N. F., Volkovski, A. R., Rodríguez-Lozano, A., Del Río, E. & Velarde, M. G. [1992] "Mutual information of chaotic self-oscillator with dissipative coupling," *Int. J. Bifurcation and Chaos* **2**(3), 669–676.

Rulkov, N. F., Tsimring, L. S. & Abarbanel, H. D. I. [1994] "Tracking unstable orbits in chaos using dissipative feedback control," *Phys. Rev.* **E50**(1), 314–324.

Shilnikov, J. F. [1970] "A contribution to the problem of the structure of an extended neighborhood of a rough equilibrium state of saddle-focus type," *Math. USSR Sbornik* **10**, 91–102.

Takens, F. [1981] "Detecting strange attractors in turbulence," in *Dynamical Systems and Turbulence* Lecture Notes in Mathematics **898**, eds. Rand, D. A. & Young, L. S. (Springer-Verlag, New York), pp. 366–381.

Volkovski, A. R. & Rulkov, N. F. [1988] "Using one dimensional mapping for the experimental study of chaotic dynamics of a self-oscillator," *Sov. Teck. Phys. Lett.* **14**, 656–659.